Journal Pre-proof

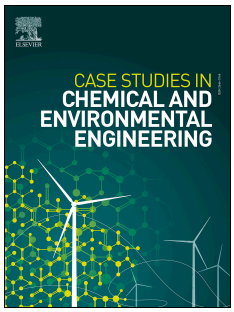

From Waste to Resource: King Coconut Biochar as a Green Adsorbent for Bisphenol A Removal

Hashinika Matharage, Mahesh Jayaweera, Nilanthi Bandara, Jagath Manatunge, Daham Jayawardana, Janith Dissanayake

PII: S2666-0164(25)00168-9

DOI: https://doi.org/10.1016/j.cscee.2025.101261

Reference: CSCEE 101261

To appear in: *Case Studies in Chemical and Environmental Engineering*

Received Date: 2 February 2025

Revised Date: 13 June 2025

Accepted Date: 16 July 2025

Please cite this article as: H. Matharage, M. Jayaweera, N. Bandara, J. Manatunge, D. Jayawardana, J. Dissanayake, From Waste to Resource: King Coconut Biochar as a Green Adsorbent for Bisphenol A Removal, *Case Studies in Chemical and Environmental Engineering*, https://doi.org/10.1016/j.cscee.2025.101261.

From Waste to Resource: King Coconut Biochar as a Green Adsorbent for Bisphenol A Removal

Hashinika Matharage*, Department of Civil Engineering, University of Moratuwa, Moratuwa 10400, Sri Lanka
dinukshimatharage@gmail.com

Mahesh Jayaweera, Department of Civil Engineering, University of Moratuwa, Moratuwa 10400, Sri Lanka
mahesh@uom.lk

Nilanthi Bandara, Department of Forestry and Environmental Science, University of Sri Jayewardenepura, Nugegoda 10250, Sri Lanka
nilanthi@sjp.ac.lk

Jagath Manatunge, Department of Civil Engineering, University of Moratuwa, Moratuwa 10400, Sri Lanka
manatunge@uom.lk

Daham Jayawardana, Department of Forestry and Environmental Science, University of Sri Jayewardenepura, Nugegoda 10250, Sri Lanka
daham@sci.sjp.ac.lk

Janith Dissanayake, Newnop Co. Ltd, 2209, 22nd Floor, Building A, 58-1, Giheung-Ro, Giheung-Gu, Yongin-Si, Gyeong-gi-Do, South Korea
Department of Civil and Environmental Engineering, Seoul National University, 1 Gwanak-Ro, Gwa-nak-Gu, Seoul, 08826, South Korea
janith1993@snu.ac.kr

* Corresponding author: Hashinika Matharage

Abstract

The widespread presence of BPA in water bodies poses significant environmental and health concerns, highlighting the need for sustainable and efficient removal technologies. This study presents an innovative approach for BPA remediation using biochar derived from king coconut shells—a readily available agricultural waste and by-product of a popular drink in many parts of Asia. Biochar pyrolyzed at 800 °C exhibited the highest removal efficiency, which was significantly enhanced to 80.1 ± 0.9% following HCl activation. Further reduction of the particle size from 1.0–4.0 mm to 75–105 µm resulted in complete (100%) removal of BPA. Batch adsorption experiments revealed optimal removal at pH 3–7, with a dosage of 5.0 g/L and an initial BPA concentration of 100.0 ppm. The adsorption process was best described by the Langmuir isotherm model (R^2 = 0.99), with a maximum capacity of 39.53 mg/g. Kinetic studies demonstrated that the pseudo-second-order model accurately represented the adsorption dynamics, implying chemisorption as the rate-limiting step. Regeneration experiments using ethanol demonstrated the reusability of the adsorbent, maintaining over 79.6% removal efficiency after five consecutive cycles. These findings highlight the effectiveness of KBC800-HCl as a sustainable and high-performance adsorbent, demonstrating the broader potential of agricultural waste valorization in environmental remediation.

Keywords

BPA removal, emerging contaminant, biochar pyrolysis, waste valorization, water treatment, adsorption isotherm, regeneration

Highlights

- King coconut shell biochar used as a green adsorbent for bisphenol A removal.
- Biochar pyrolyzed at 800°C and acid-activated showed highest bisphenol A removal.
- Adsorption followed Langmuir model, indicating monolayer surface interaction.
- Kinetic fitted pseudo-second-order model, suggesting chemisorption mechanism.

Graphical Abstract

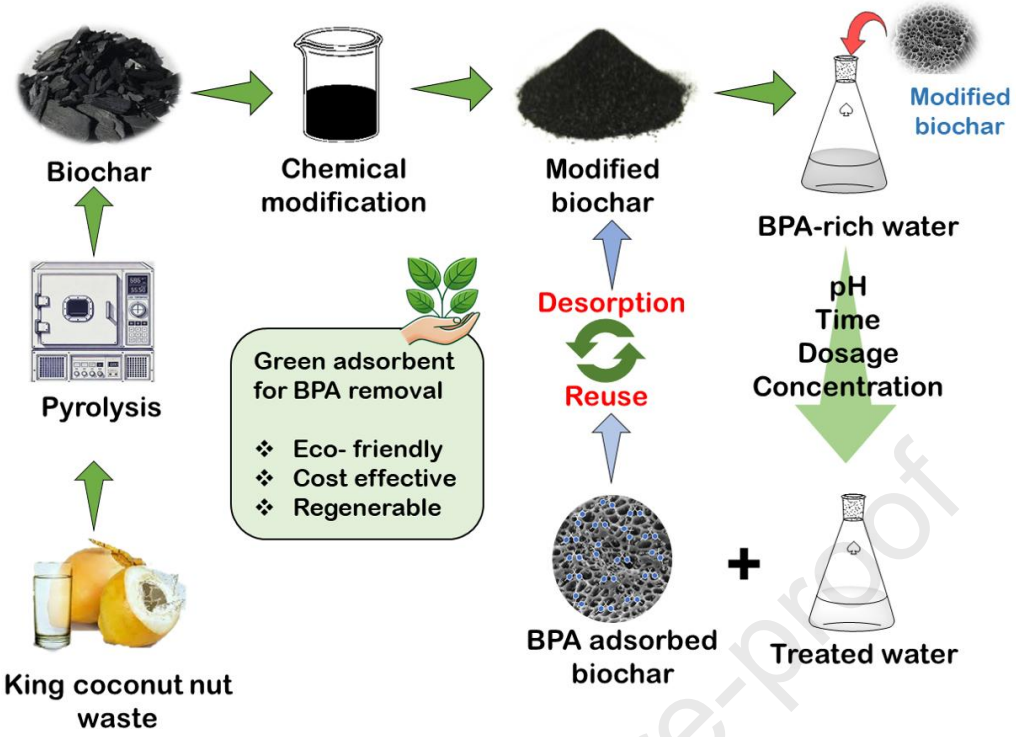

1.0 Introduction

Bisphenol A (BPA) is a non-natural organic molecule with the chemical structure of two phenol rings connected by a central carbon atom (Akash et al., 2023). It is commonly used as a precursor compound in the production of polycarbonate plastic materials and epoxy resins (Üzek et al., 2022). BPA is utilized in the manufacturing of a wide range of consumer products, encompassing baby feeding bottles, water containers, the inner coating of water pipes, beverage and food cans, toys and thermal paper (Ahmed et al., 2023; Çakıcı et al., 2023; Czarny-Krzymińska et al., 2023). The widespread utilization of BPA has led to its unavoidable dispersal into the surrounding environment.

BPA environmental releases primarily occur through migration from BPA-containing products, discharge from wastewater treatment plants, and leaching from landfill sites (Matharage et al., 2021). Consequently, it has been detected in various types of environmental waters, with BPA levels varying widely: from 17.2 mg/L in hazardous waste landfill leachate (Yamamoto et al., 2001) to 42.6 µg/L in river water (Matharage et al., 2024) and 3.5−59.8 ng/L in tap water (Santhi et al., 2012). BPA exhibits low vapor pressure (5.3×10^{-6} Pa at 25 °C); its environmental release into the air and subsequent atmospheric dispersion are deemed insignificant (Gewurtz et al., 2021). Under aerobic conditions, BPA exhibits a relatively short half-life of 2 to 7 days; however, it persists as a non-biodegradable compound under anaerobic conditions (Gewurtz et al., 2021; Matharage et al., 2024). BPA has an octanol–water partition coefficient ($\log K_{ow}$) of 3.32, indicating moderate hydrophobicity and good solubility in lipids. This lipophilic nature contributes

to its potential for bioaccumulation in aquatic organisms and raises concerns about biomagnification and long-term ecological impacts within aquatic ecosystems (Presunto et al., 2023).

The persistent presence of BPA in aquatic environments has raised significant environmental concerns, mainly due to its classification as an endocrine-disrupting chemical (EDC) (Tan et al., 2018). EDCs, including BPA, mimic or interfere with the body's hormones, potentially leading to adverse health effects in both wildlife and humans (Mpatani et al., 2021). For aquatic organisms, exposure to BPA can result in reproductive dysfunctions, developmental anomalies, and altered behavior patterns (Czarny-Krzymińska et al., 2023), thereby disrupting the integrity of aquatic ecosystems. In humans, exposure to BPA has been linked to various health problems, including cardiovascular diseases, diabetes, obesity, breast cancer, and reproductive disorders (Ahmed et al., 2023; Çakıcı et al., 2023).

Given these widespread and severe health concerns, there has been an increasing demand for effective strategies to mitigate exposure to and contamination from BPA. Strategies including coagulation/flocculation, microbial degradation, membrane filtration, advanced oxidation processes (AOPs), and adsorption have been widely employed in previous research for the removal of BPA from water (Martín-Lara et al., 2020; Shi et al., 2022). The coagulation/flocculation process is widely employed in water treatment plants to reduce pollutant concentrations (Barzegari et al., 2016). Xiaoying et al. (2009) reported BPA removal by polyaluminum chloride (PACl-Al_{13}) coagulation, achieving 32.2% removal at pH 9.0 using a dosage of 12 mg/L. Their application may introduce secondary chemical agents or generate reactive intermediates, potentially intensifying ecological risks (Zhao et al., 2024). Bacteria, fungi, and algae have shown considerable potential for BPA biodegradation (Zielińska et al., 2019). Kang and Kondo (2002) reported that *Pseudomonas* sp. and *Pseudomonas putida* achieved nearly 90% removal efficiency. However, this process can produce intermediates such as p-hydroxyacetophenone, hydroxybenzaldehyde, p-hydroxybenzoic acid, hydroquinone, and phenol, which are more toxic than BPA itself (Zielińska et al., 2019). Moreira et al. (2020) reported that the reverse osmosis (RO) membrane achieved 84% removal of BPA. Although membrane filtration is considered safe, its high energy requirements make it economically less feasible (Ahmad et al., 2023). Various AOPs have been investigated for BPA removal, with the O_3/H_2O_2 system achieving 78% efficiency, while $S_2O_8^{2-}$/UV-C and H_2O_2/UV-C systems demonstrated removal rates ranging from 52% to 85% (Moreira et al., 2020). While AOPs are highly efficient in degrading BPA, their use involves complex equipment, significant energy and chemical demands, and the risk of forming harmful by-products (Matharage et al., 2025).

The Environmental Protection Agency (EPA) has identified adsorption as one of the most efficient techniques for removing organic and inorganic substances from water (Gómez-Serrano et al., 2021). Adsorption is a competitive technique for the removal of BPA, characterized by its operational robustness, cost efficiency, high effectiveness, and lower production of hazardous by-products (Shi et al., 2022). Carbon-based materials, including activated carbon, carbon nanotubes, graphene oxide, and related derivatives, have been extensively studied in recent research as effective adsorbents for removing BPA (Zhao et al., 2024). Balarak et al. (2019) demonstrated that graphene oxide effectively adsorbed BPA, achieving a removal efficiency of 98.8 ± 0.62% at an initial concentration of 10 mg/L. Martín-Lara et al. (2020) reported that the adsorption of BPA using commercial activated carbon AC-40 achieved 93% removal at a dosage of 0.75 g/L. However, the existing carbon-based adsorbents have not fully met the urgent need for cost-effective removal of BPA (Shi et al., 2022). Consequently, the development of low-cost carbonaceous materials with enhanced adsorption capacity is of significant research interest.

In this context, utilizing biochar as an adsorbent for BPA removal offers a promising alternative. Biochar, a carbon-dense substance derived from the pyrolysis of organic biomass under limited oxygen conditions, has attracted considerable scientific interest for its potential applications in environmental remediation (Khaokomol et al., 2020). Its porous structure and high surface area make biochar an efficient adsorbent for a wide range of organic contaminants (Tan et al., 2021). Recently, biochar has been examined for its potential as a cost-effective adsorbent due to its broad accessibility, sustainable nature, robust stability, ease of synthesis, and rich content of oxygen-containing functional groups (Shi et al., 2022). These properties make it an effective replacement for conventional carbon adsorbents.

Specifically, the use of biochar derived from King coconut shells presents an innovative approach to BPA removal. King coconut, scientifically known as *Cocos nucifera* var. *aurantiaca* and originating from Sri Lanka, is esteemed for its hydrating and sweet water (Dissanayaka et al., 2023). By 2020, it had emerged as one of Sri Lanka's fastest-expanding export goods, contributing significantly to the economy with a foreign exchange revenue of Rs. 600 million (Jayasinghe et al., 2022). Factories engaged in bottling King coconut water for export generate substantial amounts of King coconut waste (Dissanayake et al., 2019). This waste, which is not commercially valuable, accumulates in factories and waste dumps (Ekanayaka et al., 2023).

This study presents a sustainable and low-cost approach to removing BPA from aqueous environments using chemically activated king coconut biochar. The novelty of this study lies in employing biochar produced from an underutilized biowaste resource—king coconut nut waste—and enhancing its adsorption performance through chemical activation for the removal of emerging contaminants such as BPA. By converting a regionally abundant agricultural waste

into a high-performance adsorbent, the research offers a practical and eco-friendly solution for water purification, particularly in resource-constrained settings.

Notably, this is the first study to investigate the application of king coconut-derived biochar for BPA remediation, thereby addressing a significant research gap in the development of sustainable adsorbent materials. To comprehensively evaluate its potential, the study examines the adsorption capacity of the modified biochar, the influence of critical operational parameters (pH, biochar dosage, and initial BPA concentration), and the adsorption kinetics to elucidate the underlying removal mechanisms. In addition to its high adsorption efficiency, the study also demonstrates the reusability of the developed biochar through regeneration experiments, confirming its applicability in repeated treatment cycles without significant loss in performance. These findings highlight the long-term feasibility and economic viability of the material for real-world water treatment applications.

Overall, this research contributes to the advancement of green remediation technologies by offering a dual environmental benefit: valorization of agricultural waste and effective mitigation of BPA contamination in water systems. The outcomes align with circular economy principles and global sustainability goals, supporting efforts to reduce pollutant exposure in aquatic ecosystems and safeguard public health.

2.0 Materials and Methods

2.1 Chemicals and Materials

Bisphenol A (4,4'-isopropylidenediphenol, 99%) was obtained from Sigma-Aldrich, USA. High-performance liquid chromatography (HPLC) grade solvents including methanol, ethanol, acetone, dichloromethane, and as well as chemicals such as hydrochloric acid (37%), sulfuric acid (98%), and nitric acid (69–72%) were procured from Sigma-Aldrich, USA. Sodium sulfate anhydrous (500 g, 99%) and sodium hydroxide (500 g, 98%) were procured from Techno Pharmchem (India). A 200.00 mg/L BPA standard solution was prepared using deionized (DI) water.

2.2 Biochar preparation

The King coconut nut waste was collected from the local suppliers. They were cleaned and cut into pieces. These pieces were uniformly dried in a drying oven at 105°C until a constant mass was achieved. After drying, the pieces were placed in a covered crucible and subjected to pyrolysis at four distinct temperatures (300 °C, 500 °C, 700 °C, and 800 °C) in a muffle furnace (Barnstead Thermolyne 6000 Muffle Furnace) (Fernando et al., 2021; Li et al., 2021; Wang et al., 2019). The biomass was heated at a rate of 7 °C per minute and maintained at that

temperature for 2 h (Matharage et al., 2025; Vithanage et al., 2015). The biochar synthesized at each temperature was left in the furnace to cool overnight. Afterward, it was rinsed with DI water to remove impurities (mainly residual ashes). It was then ground and sieved to obtain particles in the range of 1.0 to 4.0 mm. The prepared biochar samples were labelled as KBC300, KBC500, KBC700, and KBC800, correlating to their respective pyrolysis temperatures.

The biochar yield was determined using the Equation 1:

$$Biochar\ yield\ (wt\%) = \frac{W_2}{W_1} \times 100 \quad (1)$$

Where W_1 represents the dry weight of the king coconut, and W_2 denotes the weight of the resulting biochar.

2.3 Biochar modification

The King coconut biochar, processed at 800 °C, underwent separate treatments with both acidic and alkaline activators, employing solutions of 1.0 M sulfuric acid, 1.0 M hydrochloric acid, 1.0 M nitric acid, and 1.0 M sodium hydroxide, each for 24 h at ambient temperature (Araissia et al., 2023; Baharim et al., 2023). Following treatment, the adsorbents were filtered, rinsed extensively with DI water to achieve a final pH of 6–7, and then dried in a drying oven at 105 °C for 24 h. The biochar was ground into a fine powder and sieved to achieve a particle size of 75–105 µm. The samples were stored in a sealed container at room temperature until further analysis and experimental use.

2.4 Physical and chemical characterization of biochar

Proximate analysis was employed to characterize the biochar, focusing on its moisture content, ash content, volatile matter, and fixed carbon levels. The methods for proximate analysis, electrical conductivity and pH levels are summarized in the Supplementary Materials (see Supplementary Methods S1, S2, S3, S4 and S5).

The morphology and surface elemental composition of the King coconut biochar pyrolyzed at 800 °C and then activated with HCl (KBC800-HCl) were analyzed using Environmental Scanning Electron Microscopy (ESEM- Carl Zeiss, EVO 18, Secondary Electron Microscope, Germany) combined with Energy-Dispersive X-ray Spectroscopy (EDX Z1 analyser, USA).

The functional groups and chemical bonds were analyzed using Fourier Transform-Infrared Spectroscopy (FT-IR, ALPHA Bruker, Germany) in transmittance mode, covering a spectral range of 4,000 to 400 cm^{-1}, with samples prepared as KBr pellets.

The phase of KBC800-HCl was determined through X-ray Powder Diffraction (XRD-D8, ECO, Advance Bruker Diffractometer with filtered Cu Kα radiation, Germany) wavelength 1.5406 Å, at 2θ range of 10–80° and scanning speed of 2° (2θ) per minute.

Differential Scanning Calorimetry (DSC) combined with Thermogravimetric analysis (TGA) was conducted with the SDT Q600 V20.9 Build 20 (TA Instruments, USA) using nitrogen as the carrier gas and heating rate at 10.00 °C/min to 1200.00 °C.

2.5 Batch adsorption experiments

Batch adsorption experiments were conducted to evaluate the performance of each biochar in removing BPA from aqueous solution. In a typical experiment, 0.50 g of biochar and 100 mL of 100 mg/L BPA solution (pH 6–7) were placed in 250 mL conical flasks and shaken at 150 rpm for 2 hours at 30 °C using a rotary shaker.

To evaluate the effect of different parameters on BPA removal and identify the optimal experimental conditions, a series of preliminary tests were conducted by varying solution conditions. These investigations were carried out using KBC800 biochar activated with HCl (KBC800-HCl).

1) The effect of initial BPA concentrations (50.00–200.00 mg/L) on removal efficiency were assessed using 100 mL solutions with 0.5 g adsorbent, pH 6–7, 120 min contact time, at 30 °C.
2) The effect of contact time (10–100 min) at 10-minute intervals on BPA removal was studied using 0.5 g of biochar in 100 mL of 100.00 mg/L BPA solutions at 30 °C and pH 6–7.
3) The effect of initial pH (3–11) on BPA adsorption was investigated in 100 mL of 100 mg/L BPA solutions, with the pH adjusted using 0.1 M HCl or 0.1 M NaOH before adding KBC800-HCl.
4) The effect of adsorbent dosages (1.0–10.0 g/L) on BPA removal was evaluated using 100 mL of 100 mg/L BPA solution at 30 °C and pH 6–7.

The concentration of BPA before and after adsorption were measured using a UV-Vis spectrophotometer (GENESYS 10S UV-VIS, Thermo Scientific) at a wavelength of 277 nm and

Gas Chromatography/Mass Spectrometry (GC-MS), employing the Thermo Scientific GC (Trace 1300) coupled with a MS (ISQ 7000 Single Quadrupole Mass Spectrometer). All tests were performed in triplicate.

The adsorption capacity and the removal efficiency percentage were determined using Equations 2 and 3, respectively.

$$q_e = \frac{C_0 - C_e}{M} \times V \quad (2)$$

$$RE = \frac{C_0 - C_e}{C_0} \times 100 \quad (3)$$

Where q_e represents the quantity of BPA adsorbed (mg/g), C_0 is the initial concentration of the adsorbate (mg/L), C_e is the equilibrium concentration of the adsorbate (mg/L), V is the volume of the solution (L), and M is the mass of the adsorbent (g). RE represents the percentage of BPA removal efficiency.

The BPA extraction and analysis using GC-MS followed the procedures outlined in Matharage et al. (2024) and ASTM D7065-17 standard test method (ASTM, 2018) with modifications. The GC operating parameters and quality assurance and quality control procedures are outlined in the Supplementary Materials (see Supplementary Method S6 and S7, respectively).

2.6 Determination of point of zero charge (pH_{PZC}) of KBC800-HCl

The point of zero charge (pH_{PZC}) for KBC800-HCl was evaluated through the pH drift technique, following the method outlined by Jedynak and Charmas. (2024) and Santana et al. (2017) with modifications. The procedure for determining the pH_{PZC} is summarized in the Supplementary Materials (see Supplementary Methods S8). The final pH (pH_f) of the suspensions was plotted against the initial pH (pH_i). The pH_{pzc} is identified as the pH at which the curve intersects the line where the initial pH equals the final pH (Santana et al., 2017).

2.7 Mathematical modeling

2.7.1 Isotherm studies

The equilibrium data obtained were evaluated using the Langmuir, Freundlich, Dubinin–Radushkevich (D–R), and Temkin isotherm models. The linearized forms of these models were fitted to the experimental data using linear regression in OriginPro-2021. The model that showed the highest correlation coefficient (R^2) was considered the best fit to describe the adsorption behavior of KBC800-HCl for BPA removal.

The linear form of the Langmuir model is expressed in Equation 4 (Inyinbor et al., 2016). The Langmuir isotherm is characterized by the dimensionless separation factor (R_L), as shown in Equation 5.

$$\frac{C_e}{q_e} = \frac{1}{q_m} C_e + \frac{1}{K_L q_m} \quad (4)$$

$$R_L = \frac{1}{1 + C_0 K_L} \quad (5)$$

Where q_e is the equilibrium adsorption capacity of the adsorbent (mg/g), q_m is the maximum adsorption capacity (mg/g), C_e is the equilibrium adsorbate concentration (mg/L), K_L is the Langmuir constant (L/mg) related to the affinity of the binding sites and C_0 is the initial BPA concentration (mg/L) (Fachina et al., 2020). The R_L value determines whether the type of isotherm is unfavourable ($R_L > 1$), linear ($R_L = 1$), favourable ($0 < R_L < 1$) or irreversible ($R_L = 0$) (Balarak et al., 2019; Gómez-Serrano et al., 2021).

The linear form of the Freundlich model is presented in Equation 6 (Syala et al., 2024).

$$\ln q_e = \ln K_F + \frac{1}{n} \ln C_e \quad (6)$$

Where K_f is the Freundlich isotherm constant (mg/g), and n is the adsorption intensity. The n value serves as an indicator of the adsorption mechanism. Adsorption is considered favorable when n is between 2 and 10, moderately difficult when between 1 and 2, and poor when less than 1 (Kakavandi et al., 2013).

The linear form of the D-R model is expressed in Equation 7 (Inyinbor et al., 2016).

$$\ln q_e = \ln q_m - \beta \varepsilon^2 \quad (7)$$

Where q_m is the maximum adsorption capacity (mg/g), β is the activity coefficient (a constant related to the adsorption energy) (mol^2/kJ^2), and $\mathcal{E}$ is the Polanyi potential ($kJ^2\ mol^{-2}$). $\mathcal{E}$ and E are given by Equations 8 and 9.

$$\varepsilon = RT\ ln\left(1 + \frac{1}{C_e}\right) \quad (8)$$

$$E = \frac{1}{\sqrt{2\beta}} \quad (9)$$

Where R is the molar gas constant (J/mol K), T is the temperature (K) and E is the mean sorption energy (kJ/mol). If $E < 8$ kJ/mol, physisorption occurs, and if $8 < E < 16$ kJ/mol, chemisorption occurs (Saleh, 2022).

The Temkin model is presented in Equations 10 and 11 (Karim et al., 2024; Üzek et al., 2022).

$$q_e = \frac{RT}{b_T} ln\, A_T + \frac{RT}{b_T} lnC_e \quad (10)$$

$$B = \frac{RT}{b_T} \quad (11)$$

Where A_T is the equilibrium binding constant of the Temkin isotherm (L /g), b_T is the Temkin isotherm constant, T is the temperature (K), and B is the constant related to the heat of sorption (J/mol).

2.7.2 Kinetic studies

Kinetic modeling can elucidate the mechanisms of BPA adsorption and help determine the rate-limiting steps in the adsorption process (Inyinbor et al., 2016). The kinetic data were examined using the pseudo-first-order, pseudo-second-order, and Weber and Morris's intraparticle diffusion models. The linearized forms of the models were fitted to the experimental data using linear regression in OriginPro 2021. The linear forms of these kinetic models are expressed in Equations 12, 13, and 14, respectively.

$$\ln(q_e - q_t) = ln\, q_e - k_1 t \quad (12)$$

$$\frac{t}{q_t} = \frac{1}{k_2 q_e^2} + \frac{t}{q_e} \quad (13)$$

$$q_t = K_p t^{1/2} + C \quad (14)$$

Where q_e is the quantity of BPA adsorbed on the adsorbent at equilibrium (mg/g), q_t is the quantity of BPA adsorbed on the adsorbent at time t (min) (mg/g), k_1 is the adsorption rate constant of pseudo-first-order model (min^{-1}), and k_2 is the adsorption rate constant of pseudo-second-order model (g/mg/min). Furthermore, C is related to the thickness of the boundary layer (mg/g) and K_p (mg/g·$min^{1/2}$) is the intra-particle diffusion rate constant of Weber and Morris's intra-particle diffusion model.

2.8 Regeneration studies

Batch adsorption-desorption tests were performed to assess the efficacy of the adsorbent in the removal of BPA, focusing on its regeneration and desorption capabilities. The desorption and regeneration of KBC800-HCl were conducted over five consecutive cycles. Desorption was achieved by washing the KBC800-HCl with various solutions, including ethanol, methanol, 50% ethanol, 50% methanol, 0.1 M HCl, and 0.1 M NaOH (Fachina et al., 2020).

The batch experiments were carried out by employing 0.50 g of KBC800-HCl in 100 mL of BPA solution with a 100 mg/L concentration, and the contact time was 60 minutes at 30 ºC. The stirring speed was set at 150.0 rpm. Following the adsorption, KBC800-HCl was allowed to settle at the flask bottom before removing the supernatant. The KBC800-HCl was rinsed with DI water and oven-dried for 3 hours at 70°C. Subsequently, 100 mL of the regenerating solution was introduced to the KBC800-HCl and placed on the rotary shaker at 150 rpm for 60 minutes. The regeneration solution was decanted, and the KBC800-HCl solid underwent two washes with DI water, followed by decanting. The adsorbent-containing flask was oven-dried until a stable weight was reached. The weight of the flask was noted prior to commencing a subsequent adsorption and desorption cycle. Throughout the process, the weight reduction of KBC800-HCl was minimized (less than 0.01 g). The BPA adsorptions were determined after each adsorption cycle, and this entire procedure was repeated for five regeneration cycles.

3.0 Results and Discussion

3.1 Biochar preparation

Biochar yields reduced with increasing pyrolysis temperatures, as higher temperatures typically lead to greater decomposition of organic components within the biomass by creating more favorable sites (Wantaneeyakul et al., 2021). At 300 °C, the biochar yield was 55.05 ± 0.38 wt%, significantly higher than at 500 °C (46.32 ± 0.64 wt%) and 700 °C (38.73 ± 0.39 wt%). This trend is attributed to the increased decomposition within the elevated temperature range of 500−700 °C. The impact of temperature on biochar yield diminishes from 500 to 600 °C because primary fractions of hemicellulose, cellulose, and some lignin have already decomposed by 500 °C. At a pyrolysis temperature of 800 °C, biochar yield further reduced to 34.18 ± 0.32 wt%.

The BPA removal efficiency of biochar also varied with pyrolysis temperature. Prior to chemical activation, the BPA removal percentages for KBC300, KBC500, KBC700, and KBC800 were 42.0 ± 1.2%, 52.1 ± 1.3%, 60.2 ± 1.5%, and 70.1 ± 0.9%, respectively. Biochar produced by pyrolysis at 800 °C demonstrated superior effectiveness as an adsorbent for BPA removal compared to the other adsorbents. With increasing pyrolysis temperatures, the carbon content in the biochar increased as a result of the decomposition of oxygenated and nitro groups (Wathudura et al., 2020). Choi and Kan (2019) demonstrated that the development of porous structures in biochar, as well as its surface area, improved significantly with higher pyrolysis temperatures. Similarly, Wang et al. (2019) noted an increment in the pore volume of biochar corresponding to higher pyrolysis temperatures. Therefore, elevating the pyrolysis temperature facilitated an increase in both the pore volume and surface area of the biochar, thereby improving the availability of adsorption sites for BPA (Chen et al., 2017). Based on its high

adsorption capacity, the biochar produced at 800 °C was selected as the most suitable adsorbent for subsequent adsorption experiments.

3.2 Biochar modifications

Chemical activation through acid and alkali treatments has been shown to significantly improve the physicochemical properties of biochar. Such treatments enhance or generate porosity, increase pore volume, expand surface area, and boost fixed carbon content (Bushra & Remya, 2020). This improvement results from the removal of contaminants from the biochar surface, including mineral ash, metals, organic compounds, and volatile carbon (Ajien et al., 2023). After chemical activation, BPA removal efficiency improved to 74.1 ± 1.2% with NaOH, 75.7 ± 0.8% with H_2SO_4, 76.4 ± 1.1% with HNO_3, and 80.1 ± 0.9% with HCl. This improvement translates into an increase in the percentage of BPA removal of 4.1%, 5.6%, 6.3%, and 10.0% with NaOH, H_2SO_4, HNO_3, and HCl, respectively. These values are in comparison to the performance of the unmodified KBC800. Therefore, KBC modified with HCl showed the highest BPA removal efficiency among the tested materials. Ajien et al. (2023) elaborated that acid activation of biochar leads to the removal of O, S and H, which in turn enhances the aromaticity while reducing aliphatic properties. Hence, the acid modification of biochar enhanced BPA adsorption via π-π electron donor/acceptor interactions. Vithanage et al. (2015) reported that the surface area of biochar increased 285 times due to sulfuric acid activation.

Furthermore, for KBC800 activated with HCl, reducing the particle size from 1.0–4.0 mm to 75–105 µm enhanced the BPA removal efficiency from 80.1 ± 0.9% to 100%. This enhancement in removal efficiency is attributed to the increased surface area. Based on these findings, the biochar produced at 800 °C, chemically activated with HCl, and with a particle size of 75–105 µm was selected for subsequent adsorption experiments, as it achieved complete removal of BPA under the tested conditions.

3.3 Physical and chemical characterization of biochar

The proximate composition of king coconut nuts, including moisture, volatile matter, ash, and fixed carbon content, is presented in Table 1. The high volatile matter and fixed carbon contents suggest strong potential for efficient thermal decomposition and high carbon yield during pyrolysis. The previous study by Dissanayake et al.(2019) reported that the king coconut nut waste contains 83.23 ± 0.38 wt% volatile matter, 6.06 ± 0.34 wt% ash, and 10.61 ± 0.05 wt% fixed carbon. The type of pyrolysis process used significantly impacts the levels of volatile compounds and carbon content in the material. Slow pyrolysis leads to fewer volatile substances and more fixed carbon than fast pyrolysis (Maia et al., 2011). As a result, carbon levels increase

through processes such as dehydration, decarboxylation, and condensation (Bushra & Remya, 2020).

The biochar produced at different temperatures showed significantly high electrical conductivity and alkaline pH. Conductivity exhibited a marked increase, from 1.60 ± 0.04 mS/cm for KBC 300 to 12.86 ± 0.06 mS/cm for KBC 800. The pH of KBC 300 was observed to be 6.56 ± 0.01, increasing progressively with higher carbonization temperatures to reach 10.47 ± 0.02 for KBC 800. This high conductivity is attributed to substantial levels of potassium (K) and other cations within the king coconut biochar (Dissanayake et al., 2019). The abundance of potassium in the biochar was also confirmed by EDX analysis of the KBC800-HCl. An elevated pH level in biochar indicates a higher concentration of alkaline salts or minerals (such as K, Ca, Mg and Na) within biochar (Mujtaba et al., 2021). The alkaline cations in the biomass are significantly conserved within the biochar due to the reduction of C, H, and O as pyrolysis progresses.

Figure 1a and 1b display the SEM images of KBC800-HCl. The SEM images showed that KBC800-HCl exhibited a honeycomb-shaped porous structure and a large number of well-defined macro and micro-pores with clear pore walls. The porous structure is relatively regular and there are few impurities in the pores. As the pyrolysis temperature increases, the residual biomass undergoes gradual decomposition, and the elimination of volatile compounds enhances the pore volume. Generally, high-temperature biochar is characterized by porous structures with a large surface area (Li & Chen, 2018). There are no observable morphological differences in KBC800-HCl before and after the adsorption of BPA. This absence of visible changes might be attributed to BPA adsorption onto the inner walls of the tube-like structure, which makes morphological changes not readily visible from the surface. Garikoé et al. (2022) similarly reported the absence of discernible morphological differences in SEM images following the adsorption of BPA.

The EDAX analysis of KBC800-HCl shows that surface was primarily comprised of carbon (C) (67.14 wt.%), oxygen (O) (8.94 wt.%), potassium (K) (11.75 wt.%), chlorine (Cl) (4.30 wt.%), silicon (Si) (3.33 wt.%), sodium (Na) (1.74 wt.%), calcium (Ca) (1.63 wt.%), magnesium (Mg) (0.69 wt.%) and phosphorus (P) (0.49 wt.%). Furthermore, the EDX analysis indicates an 18.63% increase in the weight percentage of carbon (C) after the BPA adsorption (BPA-KBC800-HCl). The EDAX image of KBC800-HCl and BPA-KBC800-HCl are provided in the Supplementary Materials (see Figure S1 and Figure S2).

The diffractogram exhibited a broad, scattered peak within the range of 2Θ = 20–28°, characterized as graphitic carbon (Jafer et al., 2019). The broad and scattered peaks suggest that the analyzed samples exhibit low crystallinity and an amorphous nature. The three broad

diffraction peaks at approximately 2θ =9–15°, 20–28°, and 40–45°, correspond to the (110) plane with an interlayer spacing of 0.74 nm, the (002) plane with an interlayer spacing of 0.36 nm and the (100) plane with an interlayer spacing of 0.21 nm, respectively (Shi et al., 2022). These are the characteristic peaks of amorphous carbons (Adorna Jr et al., 2020). Figure 2 displays the Diffractogram of KBC800-HCl.

The TGA and DSC curves for KBC800-HCl under a nitrogen atmosphere are presented in Figure 3. These curves reveal distinct thermal behaviors due to variations in composition. The decomposition of KBC800-HCl predominantly occurred between 200 and 568 °C, with the highest mass loss rate reaching 1.61%/min from 551−557 °C. Analyzing the biochar through TGA reveals three distinct stages of mass loss. The initial mass loss of 20.5 wt.% observed between 25 and 100 °C is attributed to moisture evaporation. The most substantial loss, accounting for 63.8 wt.%, occurred between 270−560 °C corresponding to the conversion and combustion of the carbon-based structure into CO_2 (Araissia et al., 2023). A final minor loss of 6.0 wt.% is associated with the presence of a well-structured carbon network. In summary, this biochar, categorized as an amorphous carbon-rich material, experienced a total mass loss of 92.0 wt.%, leaving an 8.0 wt.% residue, which is attributed to the residual metal content from the original biomass (Araissia et al., 2023). The shoulder observed in the TGA curve (200−400 °C) indicates simultaneous degradation of cellulose and hemicellulose (Shariff et al., 2016). Beyond 400 °C, mass loss is attributed to lignin degradation and material carbonization (Choi & Kan, 2019; Wantaneeyakul et al., 2021).

In the analysis of DSC curves, the heat flow measurements reveal an initial endothermic process between 25 °C and 100 °C. Subsequently, an exothermic fluctuation is observed in the temperature range of 400 to 600 °C. Towards the end of the curve, another exothermic phenomenon is evident around 450 °C. This pattern is attributed to the evaporation of water and light volatiles at the first peak, followed by the decomposition of hemicellulose, cellulose, and lignin at the second peak (Boumanchar et al., 2017).

The characteristic peaks of BPA, KBC800-HCl, and BPA-adsorbed KBC800-HCl (BPA-KBC800-HCl) were observed in the FTIR spectra in the range of 4,000–400 cm^{-1}. In Figure 4, the 3401 cm^{-1} broad band observed in the pure BPA spectrum is attributed to the O—H stretching of self-hydrogen-bonded OH groups. The doublet appearing at 3065 and 3026 cm^{-1} is the result of the stretching vibrations of the aromatic CH groups. Moreover, the CH_3 group exhibits its characteristic asymmetric and symmetric stretching vibrations at 2969 and 2873 cm^{-1}, respectively. The peak at 1606 cm^{-1} is related to the skeletal vibration of aromatic C=C bonds (Xu et al., 2012).

The peak detected at 439 cm^{-1} in KBC800-HCl and at 443 cm^{-1} in BPA-KBC800-HCl can be assigned to the C—Cl stretching vibration associated with the presence of organochlorine compounds within the KBC800-HCl (Mujtaba et al., 2021). The peak at 1569 cm^{-1} in the KBC800-HCl is related to the stretching vibrations of C=C in aromatic rings, which are indicative of the aromatic structure of biochar (Gámiz et al., 2019; Xu et al., 2012). As biochar undergoes pyrolysis, it becomes increasingly aromatic and carbonaceous (Janu et al., 2021). Therefore, it also confirms the presence of aromatic structure in the KBC800-HCl.

Following the adsorption of BPA onto KBC800-HCl, a characteristic broad band appeared at 3791 cm^{-1} in the FTIR spectrum, providing conclusive evidence of BPA adsorption onto KBC800-HCl. When BPA is adsorbed onto the biochar surface, the interaction with the biochar may cause modifications in the hydrogen bonding or molecular conformation of BPA, shifting the O—H stretching vibration peak to a higher wavenumber, such as 3791 cm^{-1}. The peak associated with the skeletal vibration of the aromatic C=C bonds shifted from 1606 to 1566 cm^{-1} and broadened upon adsorption. These new peaks that appeared in the BPA-KBC800-HCl confirm the adsorption of BPA onto the KBC800-HCl.

3.4 Effect of contact time and initial concentration on BPA removal

The adsorption process is segmented into two phases: an initial rapid phase within the first 40 minutes, followed by a slower phase that extends to equilibrium at 60 minutes. This rapid phase is facilitated by the abundance of active binding sites available on the surface of the adsorbent (Balarak et al., 2019). However, as the process progresses into the second phase, the availability of free-binding sites is reduced. This leads to a slower adsorption rate and decreased effectiveness due to increased competition among the BPA molecules. The amount of BPA adsorbed over the contact time range of 10 to 100 minutes and the initial BPA concentration of 50.0 to 200.0 mg/L is shown in Figure 5a.

The removal of BPA gradually increased during 50.0–100.0 mg/L due to the sufficient adsorption sites. The adsorption capacity was close to the maximum when the concentration was 100.0 mg/L. As the BPA concentration surpassed 100 mg/L, a decline in the adsorption percentage was observed. In contrast, when BPA concentrations were below 100.0 mg/L, retention was higher because the pores on the KBC800-HCl surface were almost fully occupied. However, at high BPA concentrations, the pores on the KBC800-HCl surface became saturated, causing some BPA to remain unadsorbed.

At an initial concentration of 50.0 mg/L, the removal efficiency of BPA is 99.99 ± 0.01%. When the concentration increased to 100.0 mg/L, the removal efficiency reached 100.00%. However,

as the concentration increased to 125.0 mg/L, the removal efficiency slightly decreased to 99.96 ± 0.01%. Subsequently, at concentrations of 150.0 and 200.0 mg/L, the removal efficiencies dropped to 99.45 ± 0.02% and 98.16 ± 0.02%, respectively (Figure 5b).

3.5 Effect of adsrobent dosage on BPA removal

Initially an increase in KBC800-HCl dosage enhanced BPA removal percentage. At a dosage of 1.0 g/L, BPA removal was 30.4 ± 1.0%. Increasing the dosage to 3.0 g/L raised removal to 84.1 ± 0.5%, and at 5.0 g/L, BPA removal reached 100.0%. When the dosage of biochar was further increased to 8.0 g/L and then to 10.0 g/L, the removal rate remained constant at 100%.

The increase in BPA removal percentage can be attributed to the higher amount of KBC800-HCl, which expands the specific surface area available for adsorption and increases the number of active adsorption sites (Balarak et al., 2019). Simultaneously, the individual adsorption capacity of BPA by KBC800-HCl may decrease at higher adsorbent dosages. This occurs because, in situations where solutes are limited, an excess of adsorbent not only competes for solutes but also interferes with the availability of effective adsorption sites on the biochar surface, leading to overlap (Wang & Zhang, 2020). The optimal dosage was chosen as 5.0 g/L as the BPA removal percentage became 100%. The effect of the adsorbent dosage on the removal of BPA is illustrated in Figure 5c.

3.6 Effect of initial solution pH on BPA removal

The observations indicate a 100% BPA adsorption within the acidic pH range, followed by a decrease from pH 7 to pH 9 and a further decline in basic pH conditions. The BPA removal was decreased from complete removal to 84.8 ± 0.5% as the solution pH increased from pH 7 to pH 9. As the solution pH was further increased to 11, the BPA removal efficiency dropped to 35.6 ± 0.9%. The optimal percentage of BPA removal was observed at pH 3–7. The impact of the initial solution pH on BPA removal within a contact time range of 10 to 100 minutes is illustrated in Figure 6a.

This pattern is likely influenced by the pKa value of BPA, where hydroxyl ions compete with BPA molecules for active sites on biochar at basic pH (Balarak et al., 2019). The initial rapid adsorption is attributed to abundant active sites and a potent driving force, which facilitates rapid BPA transfer onto the biochar's surfaces and pores. However, a subsequent decrease in adsorbed BPA suggests that there are fewer available sites and a weaker driving force. At a pH below 8, BPA exists in its molecular form (Borrirukwisitsak et al., 2012). The initial deprotonation occurred around pH 8, followed by the second deprotonation around pH 9 (Chang et al., 2012). Following deprotonation, the majority of BPA molecules were primarily converted into mono- or

divalent anions (Xu et al., 2012). In such scenarios, the adsorbent also acquires a negative charge. Therefore, the presence of repulsive electrostatic forces between the adsorbent and the BPA could explain the decrease in the removal of BPA under highly alkaline pH conditions (Fachina et al., 2020; Jafer et al., 2019). Choi and Kan (2019) explained that the strong adsorption of BPA onto biochar in the pH range of 3 to 5 is believed to be predominantly due to π-π interactions and hydrophobic forces, given the neutral charge of BPA and the hydrophobic characteristics of biochar. Since BPA removal is 100% at pH 3, 5, and 7, adjusting the solution pH is not required for the adsorption process. Therefore, neutral pH is considered the ideal level for BPA removal.

3.7 Point of zero charge (pH_{PZC}) of KBC800-HCl

The surface charge and chemical properties of an adsorbent in water undergo significant changes with pH, making it crucial to ascertain the point of zero charge (pH_{zpc}) (Phuong & Loc, 2022). The pH_{pzc} of KBC800-HCl was determined to be 6.8, as shown in Figure 6b. This value signifies the pH at which the surface of KBC800-HCl achieves overall electrical neutrality. Below this pH, the surface typically carries a positive charge, whereas above it, the surface becomes negatively charged (Martín-Lara et al., 2020; Phuong & Loc, 2022). Consequently, when the pH is below 6.8, the surface of KBC800-HCl exhibits positive charges. Conversely, negative charges develop on the KBC800-HCl surface when the pH exceeds 6.8. At a pH of 8, KBC800-HCl exhibits a negative charge on the surface because the medium's pH exceeds the pH_{zpc} of KBC800-HCl. Within the pH range of 8 to 11, both BPA and KBC800-HCl carry negative charges, resulting in a decrease in BPA adsorption. This decline is attributed to electrostatic repulsion. When pH values approach the pH_{zpc}, the adsorbent's surface charge density becomes zero, enhancing the interaction between the KBC800-HCl surface and BPA molecules, thus promoting their adsorption (Alves et al., 2019; Jedynak & Charmas, 2024).

3.8 Adsorption isotherm studies

Several types of isotherm models are frequently employed to elucidate the adsorption process, each providing unique insights into the adsorption mechanism, the surface characteristics of the adsorbent, and the potential capacity of the adsorbent for BPA. Table 2 presents the isotherm parameters for each adsorption isotherm model, while Figure 7 illustrates the BPA adsorption isotherm models.

The correlation coefficient (R^2) values determined for the Langmuir, Freundlich, Temkin, and D-R isotherms are 0.99, 0.81, 0.96, and 0.84, respectively. The R^2 value of 0.99 suggests a strong fit of the experimental data to the Langmuir model, confirming that adsorption occurs at specific homogeneous sites within the adsorbent (Syala et al., 2024). The maximum adsorption capacity

(q_m) is 39.53 mg/g. It suggests that the KBC800-HCl has a relatively high capacity for the BPA under the studied conditions. The K_L value is 25.30 which indicates a stronger affinity between BPA and KBC800-HCl. The R_L value signifies that the adsorption process is highly favorable, as R_L falls within the range $0<R_L<1$ (Üzek et al., 2022).

It is evident from the Freundlich isotherm results that the n value is between 2 and 10, indicating that the adsorption of BPA onto KBC800-HCl is favorable. The mean free energy of adsorption (E) is 10.93 kJ/mol, as determined by the results of the Dubinin-Radushkevich adsorption isotherm. This value falls within the range of 8 to 16 kJ/mol, which typically indicates that the adsorption mechanism in this system is predominantly chemisorption (Al-Musawi et al., 2022). However, the R^2 values suggest that the experimental data do not align with the Freundlich and Dubinin-Radushkevich adsorption isotherm models.

The R^2 of 0.96 suggests that the Temkin isotherm model aligns more closely with the experimental data than the Freundlich and Dubinin-Radushkevich isotherms. The A_T is related to the maximum binding energy of the adsorption process. A high A_T value, such as 9.90×10^3 L/g, suggests that the initial adsorption energy is significant. The B value in the Temkin isotherm is related to the heat of adsorption; it indicates how the adsorption energy changes as the coverage of the adsorbent surface increases (Ahmed et al., 2023). The B value of 3.74 suggests a moderate change in the heat of adsorption as the surface coverage increases. The b_T value is 673.57 J/mol ($b_T > 1$ J/mol), confirming that the adsorption process is exothermic (Hayoun et al., 2021).

3.9 Kinetic stuides

The pseudo-first-order kinetic model for BPA adsorption is presented in Figure 8a. The first-order rate constant (k_1) was identified as 0.13 min^{-1}, with a R^2 value of 0.89. A mismatch was observed between the experimentally measured equilibrium adsorption capacity (q_e(exp)), recorded as 19.96 mg/g, and the theoretical value calculated (q_e(cal)), which was only 9.94 mg/g. The low R^2 value and the discrepancies between the experimental and theoretical adsorption capacities highlight the inadequacy of the pseudo-first-order model in accurately describing the kinetic behavior of BPA adsorption.

Figure 8b displays the pseudo-second-order kinetic model for BPA adsorption. The graph of t/q_t versus t yields a straight line with a high R^2 value of 1.0. Moreover, q_e(cal) of 20.16 mg/g closely matches the q_e(exp) of 19.96 mg/g. These findings suggest that the pseudo-second-order model more accurately represents the adsorption dynamics of BPA on KBC800-HCl, indicating that

chemisorption is the critical rate-limiting step in the BPA adsorption process. Table 3 displays the outcomes of fitting the experimental data to three different kinetic models.

Figure 8c presents the intraparticle diffusion model. The data reveal a pattern of multilinearity, showing that the adsorption process occurs in two distinct phases. Initially, there is rapid adsorption in the first phase, where the BPA is rapidly taken up by the KBC800-HCl. This phase is followed by a slower adsorption rate in the second phase. The first rapid adsorption is likely due to the chemisorption between BPA and KBC800-HCl (Supong et al., 2019). After this phase, the process slows down, likely because the adsorption starts to depend more on the slower movement of BPA molecules into the internal parts of the KBC800-HCl, a process called intraparticle diffusion (Martín-Lara et al., 2020).

The data presented in Figure 8d shows that the plotted lines do not intersect at the origin, indicating that intraparticle diffusion is not the rate-limiting step. Furthermore, the C value, which is derived from the y-intercept in the plot, was found to be nonzero, highlighting that intraparticle diffusion does not dominate the BPA adsorption mechanism on KBC800-HCl.

3.10 Regeneration stuides

For large-scale industrial treatment, adsorption is challenging due to the requirement for large amounts of adsorbents, leading to increased operational costs (Ahmad et al., 2023). To minimize these costs, utilizing the adsorbent multiple times is essential. Therefore, the regeneration of the adsorbent is crucial for its economic feasibility because it significantly reduces the cost associated with the removal process (Ahmad et al., 2023). Moreover, the regeneration of adsorbents can reduce the environmental impacts resulting from the improper disposal of the adsorbents. Fachina et al.(2020) reported that the use of 50% methanol and 50% ethanol, compared to acid (0.1 M HCl) and base (0.1 M NaOH), was more favorable for the desorption process (Fachina et al., 2020).

The adsorption capacity of BPA gradually decreases over five adsorption-desorption cycles using different eluting agents, as shown in Figure 9. The efficiency of BPA removal through adsorption progressively dropped from 99.5% to 79.6% using ethanol as the eluting agent over five consecutive regeneration cycles. The ethanol solution interferes with the interaction between hydroxyl groups and aromatic rings, facilitated by hydrogen bonding and π-π interactions. This interference has consequently led to the desorption of BPA (Mpatani et al., 2021). Additionally, the efficiency of removing BPA by adsorption experienced a gradual decrease in five consecutive regeneration cycles, dropping from 99.6% to 74.2% with HCl, from 98.5% to 71.5% with NaOH, from 99.0% to 72.1% with methanol, from 97.2% to 65.2% with

50% ethanol, and from 96.5% to 66.1% with 50% methanol as eluting agents, respectively. Tursi et al. (2018) have explained that NaOH solution could neutralize the surface of the adsorbent, potentially disrupting the hydrophobic interactions between BPA and the adsorbent. All eluting agents achieved a removal efficiency greater than 65.0%, even after five regeneration cycles. The findings of the regeneration study indicated that ethanol is the most effective eluting agent for regenerating KBC800-HCl.

3.10 Possible mechanism

The adsorption behavior of BPA onto biochar is strongly influenced by the structural characteristics developed during the pyrolysis process. As the pyrolysis temperature increases, significant changes occur in the carbon structure, particularly the development of aromatic domains. An increase in pyrolysis temperature results in a higher accumulation of aromatic benzene rings within the biochar, which in turn enhances its ability to act as a superior π-electron acceptor (Wang et al., 2019). Similarly, Khaokomol et al. (2020) and Das et al. (2015) explained that elevated temperatures led to the formation of biochar with larger aromatic domains and more organized structures. Since BPA possesses strong π-electron donating capabilities, this dynamic significantly bolsters the π–π electron donor/acceptor interactions between biochar and BPA, and these interactions are likely the dominant mechanism in this system. Chen et al. (2017) further corroborate that these π-π electron donor/acceptor interactions are crucial in mediating the adsorption efficiency of BPA onto biochar. However, the adsorption process cannot be attributed to a single mechanism; rather, it involves the simultaneous contribution of multiple mechanisms acting in parallel to govern the overall adsorption behavior.

In this system, the pore-filling mechanism may also play an important role in the adsorption of BPA. The increase in pyrolysis temperature promotes the development of surface area and pore volume, primarily due to the release of volatile matter, resulting in a more porous biochar structure. This enhancement in porosity facilitates the physical accommodation of BPA molecules within the internal pore network (Shi et al., 2022; Wang et al., 2019). As a result, the pore-filling effect contributes to rapid adsorption, particularly during the initial stages of contact, leading to a higher initial removal rate (Araujo et al., 2024).

Hydrophobic interactions are also likely to facilitate BPA adsorption by promoting affinity between the hydrophobic moieties of BPA and the hydrophobic surface of KBC800-HCl (Choi & Kan, 2019). Electrostatic interactions are unlikely to influence the adsorption of BPA onto KBC800-HCl, given that the pH_{pzc} of the material is 6.8. Although BPA contains two hydroxyl groups, it predominantly remains in its neutral molecular form at neutral pH. It stays protonated under acidic conditions and begins to deprotonate only under basic conditions (pH > 7) (Hayoun et al., 2021). As such, electrostatic interactions are not considered a contributing factor in the

adsorption process of BPA onto KBC800-HCl. The possible mechanisms for BPA adsorption onto KBC800-HCl are illustrated in Figure 10.

4.0 Conclusions

This study demonstrates the successful development and application of chemically activated king coconut biochar (KBC800-HCl) as a high-performance adsorbent for the removal of BPA from aqueous solutions. The biochar produced at 800 °C and activated with HCl exhibited the highest adsorption efficiency, achieving 80.1% removal, which was further enhanced to complete (100%) removal upon reducing the particle size to 75–105 µm. Batch adsorption studies indicated that optimal BPA removal occurred under mildly acidic to neutral conditions (pH 3–7), with a biochar dosage of 5.0 g/L and an initial BPA concentration of 100.0 ppm.

Adsorption process was best described by the Langmuir isotherm model, indicating monolayer adsorption with a maximum adsorption capacity (q_m) of 39.53 mg/g. Kinetic data followed the pseudo-second-order model, suggesting chemisorption as the rate-limiting step. Furthermore, regeneration studies revealed good reusability, with ethanol maintaining over 79.6% removal efficiency after five cycles. The π–π electron donor/acceptor interaction, pore-filling effect, and hydrophobic interaction are the possible mechanisms involved in the adsorption of BPA onto KBC800-HCl biochar.

These findings highlight the potential of KBC800-HCl as a low-cost, efficient, and reusable adsorbent for emerging contaminant removal. The study contributes to advancing biochar-based water treatment technologies and supports broader environmental sustainability through waste valorization and resource recovery.

Appendix A. Supplementary data

Supplementary data related to this article can be found online.

Acknowledgements

The authors acknowledge the University of Sri Jayewardenepura, Sri Lanka, for essential financial support through Research Grant ASP/01/RE/SCI/2018/24, which was crucial for this research.

Author Contributions

Conceptualization: Hashinika Matharage, Mahesh Jayaweera; Methodology: Hashinika Matharage, Mahesh Jayaweera, Jagath Manatunge; Formal analysis and investigation: Hashinika Matharage; Writing - original draft preparation: Hashinika Matharage; Writing - review and editing: Hashinika Matharage, Mahesh Jayaweera, Jagath Manatunge, Nilanthi Bandara, Daham Jayawardana, Janith

Dissanayake; Software: Hashinika Matharage; Funding acquisition: Nilanthi Bandara, Daham Jayawardana; Resources: Mahesh Jayaweera, Jagath Manatunge, Nilanthi Bandara, Janith Dissanayake; Supervision: Mahesh Jayaweera, Jagath Manatunge, Nilanthi Bandara, Daham Jayawardana.

Data Availability Statement

All relevant data are included in the paper or its Supplementary Information.

References

Adorna Jr, J., Borines, M., Doong, R.-A. (2020). Coconut shell derived activated biochar–manganese dioxide nanocomposites for high performance capacitive deionization. Desalination 492, 114602. https://doi.org/10.1016/j.desal.2020.114602.

Ahmad, T., Manzar, M. S., Georgin, J., Franco, D. S., Khan, S., Meili, L., Ullah, N. (2023). Development of a new hyper crosslinked resin based on polyamine-isocyanurate for the efficient removal of endocrine disruptor bisphenol-A from water. J. Water. Process. Eng. 53, 103623. https://doi.org/10.1016/j.jwpe.2023.103623.

Ahmed, A. S. A., El-Nahas, S., Ezzeldien, M. (2023). Purification of drinking water from dissolved Bisphenol A (BPA) using zinc oxide nanoparticles. Aswan Univ. J. Environ. Stud. 4, 48-68. https://doi.org/10.21608/aujes.2023.174975.1108.

Ajien, A., Idris, J., Md Sofwan, N., Husen, R., Seli, H. (2023). Coconut shell and husk biochar: A review of production and activation technology, economic, financial aspect and application. Waste Manag. Res. 41, 37-51. https://doi.org/10.1177/0734242X221127167.

Akash, M. S. H., Rasheed, S., Rehman, K., Imran, M., Assiri, M. A. (2023). Toxicological evaluation of bisphenol analogues: preventive measures and therapeutic interventions. RSC Adv. 13, 21613-21628. https://doi.org/10.1039/D3RA04285E.

Al-Musawi, T. J., Mengelizadeh, N., Ganji, F., Wang, C., Balarak, D. (2022). Preparation of multi-walled carbon nanotubes coated with $CoFe_2O_4$ nanoparticles and their adsorption performance for Bisphenol A compound. Adv. Powder Technol. 33, 103438. https://doi.org/10.1016/j.apt.2022.103438.

Alves, A. C. F., Antero, R. V. P., de Oliveira, S. B., Ojala, S. A., Scalize, P. S. (2019). Activated carbon produced from waste coffee grounds for an effective removal of bisphenol-A in aqueous medium. Environ. Sci. Pollut. Res. 26, 24850-24862. https://doi.org/10.1007/s11356-019-05717-7.

Araissia, H., Guellati, O., Abbaci, F., Harat, A., El-Haskouri, J., Begin, D., Guerioune, M., Nait-Merzoug, A. (2023). Physico-Chemical Properties of Three Synthesized Carbonaceous Nanomaterials

(CNTs, GO, Biochar) for Perspective Application: Water/Soil Treatment and Energy Storage. Eng. Sci., 3, 35. https://doi.org/10.53907/enpesj.v3i1.160.

Araujo, R. O., Anjos, O. C. d., Souza, L. K. d., Bataglion, G. A. (2024). Biochar from lignocellulosic biomass: a sustainable circular economy approach for removing organic and inorganic contaminants. Quím. Nova, 47, e-20240079. https://doi.org/https://doi.org/10.21577/0100-4042.20240079.

ASTM. (2018). Standard test method for determination of Nonylphenol, Bisphenol A, p-tert-Octylphenol, Nonylphenol Monoethoxylate and Nonylphenol Diethoxylate in environmental waters by Gas Chromatography Mass Spectrometry (ASTM D7065-17). In. West Conshohocken, PA,USA: ASTM international.

Baharim, N. H., Sjahrir, F., Taib, R. M., Idris, N., Daud, T. A. T. (2023). Removal of Crystal Violet from Aqueous Solution Using Post-treated Activation Biochar Derived from Banana Pseudo Stem. Chem. Eng. Trans. 98, 45-50. https://doi.org/10.3303/CET2398008.

Balarak, D., Ansari, H., Dashtizadeh, M., Bazi, M. (2019). Synthesis of Graphene Oxide as an Adsorbent for the Removal of Bisphenol A. J. Hum. Environ. Health Promot. 5, 98-103. https://doi.org/10.29252/jhehp.5.3.1.

Bhatnagar, A., Anastopoulos, I. (2017). Adsorptive removal of bisphenol A (BPA) from aqueous solution: A review. Chemosphere. 168, 885-902. https://doi.org/10.1016/j.chemosphere.2016.10.121.

Borrirukwisitsak, S., Keenan, H. E., Gauchotte-Lindsay, C. (2012). Effects of salinity, pH and temperature on the octanol-water partition coefficient of bisphenol A. Int. J. Environ. Sci. Dev. 3, 460. https://doi.org/10.7763/IJESD.2012.V3.267.

Boumanchar, I., Chhiti, Y., Alaoui, F. E. M. h., El Ouinani, A., Sahibed-Dine, A., Bentiss, F., Jama, C., Bensitel, M. (2017). Effect of materials mixture on the higher heating value: Case of biomass, biochar and municipal solid waste. Waste Manag. 61, 78-86. https://doi.org/10.1016/j.wasman.2016.11.012.

Bushra, B., Remya, N. (2020). Biochar from pyrolysis of rice husk biomass—characteristics, modification and environmental application. Biomass Convers. Bioref. 14, 5759–5770. https://doi.org/10.1007/s13399-020-01092-3.

Çakıcı, M., Avan, A. A., Filik, H., Kök Yetimoğlu, E. (2023). Individual and Simultaneous Electrochemical Detection of Bisphenol A and Bisphenol S in Food Samples Using Triethylenetetramine Functionalized Multi-Walled Carbon Nanotubes. Food Anal. Methods 16, 225-237. https://doi.org/10.1007/s12161-022-02409-w.

Chang, K.-L., Hsieh, J.-F., Ou, B.-M., Chang, M.-H., Hseih, W.-Y., Lin, J.-H., Huang, P.-J., Wong, K.-F., Chen, S.-T. (2012). Adsorption studies on the removal of an endocrine-disrupting compound (Bisphenol A) using activated carbon from rice straw agricultural waste. Sep. Sci. Technol. 47, 1514-1521. https://doi.org/10.1080/01496395.2011.647212.

Chen, J., Zhang, D., Zhang, H., Ghosh, S., Pan, B. (2017). Fast and slow adsorption of carbamazepine on biochar as affected by carbon structure and mineral composition. Sci. Total Environ. 579, 598-605. https://doi.org/10.1016/j.scitotenv.2016.11.052.

Choi, Y.-K., Kan, E. (2019). Effects of pyrolysis temperature on the physicochemical properties of alfalfa-derived biochar for the adsorption of bisphenol A and sulfamethoxazole in water. Chemosphere 218, 741-748. https://doi.org/10.1016/j.chemosphere.2018.11.151.

Czarny-Krzymińska, K., Krawczyk, B., Szczukocki, D. (2023). Bisphenol A and its substitutes in the aquatic environment: Occurrence and toxicity assessment. Chemosphere 315, 137763. https://doi.org/10.1016/j.chemosphere.2023.137763.

Das, D., Samal, D. P., Meikap, B. (2015). Preparation of activated carbon from green coconut shell and its characterization. J. Chem. Eng. Process Technol. 6, 1000248. https://doi.org/10.4172/2157-7048.1000248.

Dissanayaka, N. S., Dissanayake, L., Dassanayake, S. D., Udumann, S. S., Keerthisinghe, J. P., Jayalath, N., Idirisinghe, S. K., Silva, S., Gammampila, J., Janaka, R. (2023). Enhancing Sustainable Agriculture through King Coconut Husk Ash: Investigating Optimal Processing Parameters for High Potassium Content and Efficient Waste Management. Biol. Life Sci. Forum. 27, 17. https://doi.org/10.3390/IECAG2023-15802.

Dissanayake, L., Dharmakeerthi, R., Herath, I. (2019). Production and Characterization of King Coconut Waste Biochar. Paper presented at the International Symposium on Sustainable Soil Management. Soil: Underpinning life and environment, Kandy, Sri Lanka, December 5-6, 2019, https://doi.org/10.13140/RG.2.2.20650.13766.

Ekanayaka, E. M. G. N., Dissanayake, D. K. R. P. L., Udumann, S. S., Dissanayaka, D. M. N. S., Nuwarapaksha, T. D., Herath, H. M. S. K., Atapattu, A. J. (2023). Sustainable Utilization of King Coconut Husk as a Feedstock in Biochar Production with the Highest Conversion Efficiency and Desirable Properties. IOP Conference Series: Earth and Environmental Science. 1235, 012009. https://doi.org/10.1088/1755-1315/1235/1/012009.

Fachina, Y. J., Andrade, M. B. d., Guerra, A. C. S., Santos, T. R. T. d., Bergamasco, R., Vieira, A. M. S. (2020). Graphene oxide functionalized with cobalt ferrites applied to the removal of bisphenol A: ionic study, reuse capacity and desorption kinetics. Environ. Technol. 43, 1388-1404. https://doi.org/10.1080/09593330.2020.1830183.

Fernando, J. C., Peiris, C., Navarathna, C. M., Gunatilake, S. R., Welikala, U., Wanasinghe, S. T., Madduri, S. B., Jayasinghe, S., Mlsna, T. E., Ferez, F. (2021). Nitric acid surface pre-modification of novel Lasia spinosa biochar for enhanced methylene blue remediation. Groundw. Sustain. Dev. 14, 100603. https://doi.org/10.1016/j.gsd.2021.100603.

Gámiz, B., Hall, K., Spokas, K. A., Cox, L. (2019). Understanding activation effects on low-temperature biochar for optimization of herbicide sorption. Agronomy 9, 588. https://doi.org/10.3390/agronomy9100588.

Garikoé, I., Guel, B., Persson, I. (2022). Sorption of Bisphenol A as Model for Sorption Ability of Organoclays. Molecules. 27, 4343. https://doi.org/10.3390/molecules27144343.

Gewurtz, S. B., Tardif, G., Power, M., Backus, S. M., Dove, A., Dubé-Roberge, K., Garron, C., King, M., Lalonde, B., Letcher, R. J. (2021). Bisphenol A in the Canadian environment: A multimedia analysis. Sci. Total Environ. 755, 142472. https://doi.org/10.1016/j.scitotenv.2017.05.069.

Gómez-Serrano, V., Adame-Pereira, M., Alexandre-Franco, M., Fernández-González, C. (2020). Adsorption of bisphenol A by activated carbon developed from PET waste by KOH activation. Environ. Sci. Pollut. Res. 28, 24342–24354. https://doi.org/10.1007/s11356-020-08428-6.

Hayoun, B., Bourouina-Bacha, S., Pazos, M., Sanromán, M. A., Benkhennouche-Bouchene, H., Deflaoui, O., Hamaidi-Maouche, N., Bourouina, M. (2021). Production of modified sunflowers seed shells for the removal of bisphenol A. RSC Adv. 11, 3516-3533. https://doi.org/10.1039/D0RA09137E.

Inyinbor, A., Adekola, F., Olatunji, G. A. (2016). Kinetics, isotherms and thermodynamic modeling of liquid phase adsorption of Rhodamine B dye onto *Raphia hookerie* fruit epicarp. Water Resour. Ind. 15, 14-27. https://doi.org/10.1016/j.wri.2016.06.001.

Jafer, M., Ibrahim, H., Taufiq-Yap, Y. (2019). Bisphenol A Removal from Aqueous Solution Using Waste Agarwood Activated Carbon: Kinetic and Isotherm Investigation of Adsorption Process. Eurasian J. Anal. Chem. 14, 32-41.

Janu, R., Mrlik, V., Ribitsch, D., Hofman, J., Sedláček, P., Bielská, L., Soja, G. (2021). Biochar surface functional groups as affected by biomass feedstock, biochar composition and pyrolysis temperature. Carbon Resour. Convers. 4, 36-46. https://doi.org/10.1016/j.crcon.2021.01.003.

Jayasinghe, M. D., Madage, S. S. K., Hewajulige, I. G. N., Jayawardana, T. M. D. A., Halmillawewa, A. P., Divisekera, D. M. W. D. (2022). Identification of Potentially Hazardous Microorganisms and Assessment of Physicochemical Deterioration of Thermally Processed King Coconut (*Cocos nucifera* var. *aurantiaca*) Water under Different Processing Conditions in Sri Lanka. J. Food Qual. 6752088, 15. https://doi.org/10.1155/2022/6752088.

Jedynak, K., Charmas, B. (2023). Adsorption properties of biochars obtained by KOH activation. Adsorption, 30, 167–183. https://doi.org/10.1007/s10450-023-00399-7.

Kakavandi, B., Jonidi, A., Rezaei, R., Nasseri, S., Ameri, A., Esrafily, A. (2013). Synthesis and properties of Fe_3O_4-activated carbon magnetic nanoparticles for removal of aniline from aqueous solution: equilibrium, kinetic and thermodynamic studies. Iran. J. Environ. Health Sci. Eng. 10, 1-9. https://doi.org/10.1186/1735-2746-10-19.

Kang, J.-H., Kondo, F. (2002). Bisphenol A degradation by bacteria isolated from river water. Arch Environ Contam Toxicol. 43, 0265-0269. https://doi.org/https://doi.org/10.1007/s00244-002-1209-0.

Karim, M. A., Ahmed, S., Hossain, D., Hossain, M. I., Hossain, M. S., Hossain, A., Rahman, M. H., Dipti, S. S., Azad, M. A. K. (2024). Adsorption Isotherms and Kinetics Studies on Adsorption of Malachite Green onto Activated Charcoal from Aqueous Solution. J. Sci. Eng. Pap. 1, 18-25. https://doi.org/10.62275/josep.24.1000004.

Khaokomol, S., Neamchan, R., Panpradit, B., Sohsalam, P., Werner, D., Mrozik, W. (2020). Suitalbility and Cost Effectiveness of Biochars Produced from Different Agricultural Residues with Different Methods for Briquette Making as a Renewable Biofuel. https://doi.org/10.2139/ssrn.3598081.

Li, Q., Zhao, S., Wang, Y. (2021). Mechanism of Oxytetracycline Removal by Coconut Shell Biochar Loaded with Nano-Zero-Valent Iron. Int. J. Environ. Res. Public Health 18, 13107. https://doi.org/10.3390/ijerph182413107.

Li, S., Chen, G. (2018). Thermogravimetric, thermochemical, and infrared spectral characterization of feedstocks and biochar derived at different pyrolysis temperatures. Waste Manag. 78, 198-207. https://doi.org/10.1016/j.wasman.2018.05.048.

Maia, C., Madari, B. E., Novotny, E. H. (2011). Advances in biochar research in Brazil. Dyn. Soil Dyn. Plant. 5, 53-58.

Martín-Lara, M., Calero, M., Ronda, A., Iáñez-Rodríguez, I., Escudero, C. (2020). Adsorptive behavior of an activated carbon for bisphenol A removal in single and binary (bisphenol A—heavy metal) solutions. Water, 12, 2150. https://doi.org/10.3390/w12082150.

Matharage, H., Jayaweera, M., Bandara, N., Gunawardana, B. (2021). Occurrence of Bisphenol A in Bolgoda Lake Receiving Leachate from a Solid Waste Open Dump: A Silent Killer of a Healthy Ecosystem, From Innovation To Impact (FITI), Colombo, Sri Lanka. pp. 1-5, doi: 10.1109/FITI54902.2021.9833066.

Matharage, H., Jayaweera, M., Bandara, N., Jayawardana, D., Zoysa, K. (2024). Occurrence, persistence, and ecological risk of bisphenol A in surface water receiving raw leachate from a municipal solid waste open dump in Kerawalapitiya, Sri Lanka. Environ. Qual. Manag. 33, 759-770. https://doi.org/10.1002/tqem.22154.

Matharage, H., Jayaweera, M., Bandara, N., Manatunge, J., Jayawardana, D., Dissanayake, J. (2025). Fixed-bed column studies on the adsorption of bisphenol A from aqueous solutions using chemically activated king coconut biochar. Discov. Chem. Eng. 5, 9. https://doi.org/10.1007/s43938-025-00082-z.

Moreira, C. G., Moreira, M. H., Silva, V. M. O. C., Santos, H. G., Bila, D. M., Fonseca, F. V. (2020). Treatment of Bisphenol A (BPA) in water using UV/H_2O_2 and reverse osmosis (RO) membranes: assessment of estrogenic activity and membrane adsorption. Water Sci. Technol. 80, 2169-2178. https://doi.org/10.2166/wst.2020.024.

Mpatani, F. M., Han, R., Aryee, A. A., Kani, A. N., Li, Z., Qu, L. (2021). Adsorption performance of modified agricultural waste materials for removal of emerging micro-contaminant bisphenol A: a comprehensive review. Sci. Total Environ. 780, 146629. https://doi.org/10.1016/j.scitotenv.2021.146629.

Mujtaba, G., Hayat, R., Hussain, Q., Ahmed, M. (2021). Physio-chemical characterization of biochar, compost and co-composted biochar derived from green waste. Sustainability 13, 4628. https://doi.org/10.3390/su13094628.

Phuong, D. T. M., Loc, N. X. (2022). Rice straw biochar and magnetic rice straw biochar for safranin O adsorption from aqueous solution. Water 14, 186. https://doi.org/10.3390/nano6070128.

Presunto, M., Mariana, M., Lorigo, M., Cairrao, E. (2023). The Effects of Bisphenol A on Human Male Infertility: A Review of Current Epidemiological Studies. Int. J. Mol. Sci. 24, 12417. https://doi.org/10.3390/ijms241512417.

Saleh, T. A. (2022). Chapter 4 - Isotherm models of adsorption processes on adsorbents and nanoadsorbents. in Saleh, T. A. (Ed.), Interface Science and Technology , 34, pp. 99-126. Elsevier. https://doi.org/10.1016/B978-0-12-849876-7.00009-9.

Santana, G. M., Lelis, R. C. C., Jaguaribe, E. F., Morais, R. d. M., Paes, J. B., Trugilho, P. F. (2017). Development of activated carbon from bamboo (*Bambusa vulgaris*) for pesticide removal from aqueous solutions. CERNE, 23, 123-132. https://doi.org/10.1590/01047760201723012256.

Santhi, V., Sakai, N., Ahmad, E., Mustafa, A. (2012). Occurrence of bisphenol A in surface water, drinking water and plasma from Malaysia with exposure assessment from consumption of drinking water. Sci. Total Environ. 427, 332-338. https://doi.org/10.1016/j.scitotenv.2012.04.041.

Shariff, A., Aziz, N. M., Ismail, N. I., Abdullah, N. (2016). Corn cob as a potential feedstock for slow pyrolysis of biomass. J. Phys. Sci. 27, 123-137. https://doi.org/10.21315/jps2016.27.2.9.

Shi, W., Wang, H., Yan, J., Shan, L., Quan, G., Pan, X., Cui, L. (2022). Wheat straw derived biochar with hierarchically porous structure for bisphenol A removal: Preparation, characterization, and adsorption properties. Sep. Purif. Technol. 289, 120796. https://doi.org/10.1016/j.seppur.2022.120796.

Supong, A., Bhomick, P. C., Baruah, M., Pongener, C., Sinha, U. B., Sinha, D. (2019). Adsorptive removal of Bisphenol A by biomass activated carbon and insights into the adsorption mechanism through density functional theory calculations. Sustain. Chem. Pharm. 13, 100159. https://doi.org/10.1016/j.scp.2019.100159.

Syala, E., Sadik, W. A., El-Demerdash, A.-G. M., Mekhamer, W., El-Rafey, M. E. (2024). The effective treatment of dye-containing simulated wastewater by using the cement kiln dust as an industrial waste adsorbent. Sci. Rep. 14, 14589. https://doi.org/10.1038/s41598-024-64191-5.

Tan, R., Liu, R., Li, B., Liu, X., Li, Z. (2018). Typical endocrine disrupting compounds in rivers of Northeast China: occurrence, partitioning, and risk assessment. Arch. Environ. Contam. Toxicol. 75, 213-223. https://doi.org/10.1007/s00244-017-0482-x.

Tan, X.-F., Zhu, S.-S., Wang, R.-P., Chen, Y.-D., Show, P.-L., Zhang, F.-F., Ho, S.-H. (2021). Role of biochar surface characteristics in the adsorption of aromatic compounds: Pore structure and functional groups. Chin. Chem. Lett. 32, 2939-2946. https://doi.org/10.1016/j.cclet.2021.04.059.

Tursi, A., Chatzisymeon, E., Chidichimo, F., Beneduci, A., Chidichimo, G. (2018). Removal of endocrine disrupting chemicals from water: adsorption of bisphenol-A by biobased hydrophobic functionalized cellulose. Int. J. Environ. Res. Public Health 15, 2419. https://doi.org/10.3390/ijerph15112419.

Üzek, R., Şenel, S., Denizli, A. (2022). Investigation of thermodynamic, kinetic, and isothermal parameters for the selective adsorption of bisphenol A. ACS Omega 7, 18940-18952. https://doi.org/10.1021/acsomega.2c01975.

Vithanage, M., Rajapaksha, A. U., Zhang, M., Thiele-Bruhn, S., Lee, S. S., Ok, Y. S. (2015). Acid-activated biochar increased sulfamethazine retention in soils. Environ. Sci. Pollut. Res. 22, 2175-2186. https://doi.org/10.1007/s11356-014-3434-2.

Wang, F., Zeng, Q., Su, W., Zhang, M., Hou, L., Wang, Z.-L. (2019). Adsorption of Bisphenol A on Peanut Shell Biochars: The Effects of Surfactants. J. Chem. 2019, 2428505. https://doi.org/10.1155/2019/2428505.

Wang, J., Zhang, M. (2020). Adsorption characteristics and mechanism of bisphenol A by magnetic biochar. Int. J. Environ. Res. Public Health 17, 1075. https://doi.org/10.3390/ijerph17031075.

Wantaneeyakul, N., Kositkanawuth, K., Turn, S. Q., Fu, J. (2021). Investigation of Biochar Production from Copyrolysis of Rice Husk and Plastic. ACS Omega 6, 28890-28902. https://doi.org/10.1021/acsomega.1c03874.

Wathudura, P. D., Peiris, C., Navarathna, C. M., Mlsna, T. E., Kaumal, M., Vithanage, M., Gunatilake, S. R. (2020). Microwave and open vessel digestion methods for biochar. Chemosphere 239, 124788. https://doi.org/10.1016/j.chemosphere.2019.124788.

Xiaoying, M., Guangming, Z., Chang, Z., Zisong, W., Jian, Y., Jianbing, L., Guohe, H., & Hongliang, L. (2009). Characteristics of BPA removal from water by PACl-Al13 in coagulation process. J. Colloid Interface Sci. 337, 408-413. https://doi.org/10.1016/j.jcis.2009.05.052.

Xu, J., Wang, L., Zhu, Y. (2012). Decontamination of bisphenol A from aqueous solution by graphene adsorption. Langmuir 28, 8418-8425. https://doi.org/10.1021/la301476p.

Yamamoto, T., Yasuhara, A., Shiraishi, H., Nakasugi, O. (2001). Bisphenol A in hazardous waste landfill leachates. Chemosphere 42, 415-418. https://doi.org/10.1016/S0045-6535(00)00079-5.

Zhao, Y., Yang, M., Qi, K., Pan, J. (2024). The adsorption of bisphenol A by biochars modified with potassium phosphate. Desalin. Water Treat. 319, 100444. https://doi.org/https://doi.org/10.1016/j.dwt.2024.100444

Zielińska, M., Wojnowska-Baryła, I., Cydzik-Kwiatkowska, A., Zielińska, M., Wojnowska-Baryła, I., Cydzik-Kwiatkowska, A. (2019). Microbial biodegradation and metabolism of BPA. In Bisphenol A Removal from Water and Wastewater (pp. 61-78). Springer, Cham. https://doi.org/https://doi.org/10.1007/978-3-319-92361-1_4

Table 1. Proximate composition of king coconut nuts

Parameter	Value (wt %)
Moisture	29.10 ± 0.43
Volatile matter	33.45 ± 0.66
Ash	7.78 ± 0.30
Fixed carbon	29.67 ± 0.78

Table 2. Isotherm parameters

Isotherm model	Parameter	Value
Langmuir	q_m (mg/g)	39.53
	K_L (L/mg)	25.30
	R^2	0.99
Freundlich	K_F	37.33
	n	5.84
	R^2	0.81
Temkin	A_T (L/g)	9.90×10^3
	B (J/mol)	3.74
	b_T (J/mol)	673.57
	R^2	0.96
Dubinin- Radushkevich	q_m (mg/g)	36.42
	E (kJ/mol)	10.93
	β (mol^2/kJ^2)	4.18×10^{-3}
	R^2	0.84

1041 Table 3. Kinetic study parameters

kinetic model		Parameter	Value
Pseudo-first-order model	C_0=100.0 mg/L	q_e (exp) (mg/g)	19.96
		q_e (cal) (mg/g)	9.94
		k_1(min^{-1})	0.13
		R^2	0.89
Pseudo-second-order model	C_0=100.0 mg/L	q_e (exp) (mg/g)	19.96
		q_e (cal) (mg/g)	20.16
		k_2 (g/min/mg)	0.058
		R^2	1.00
Intraparticle diffusion model	C_0=100.0 mg/L		
	Stage 1	K_p (mg/g·$min^{1/2}$)	0.44
		C (mg/g)	17.13
		R^2	0.99
	Stage 2	K_p (mg/g·$min^{1/2}$)	0.002
		C (mg/g)	19.93
		R^2	0.57

1042

1043

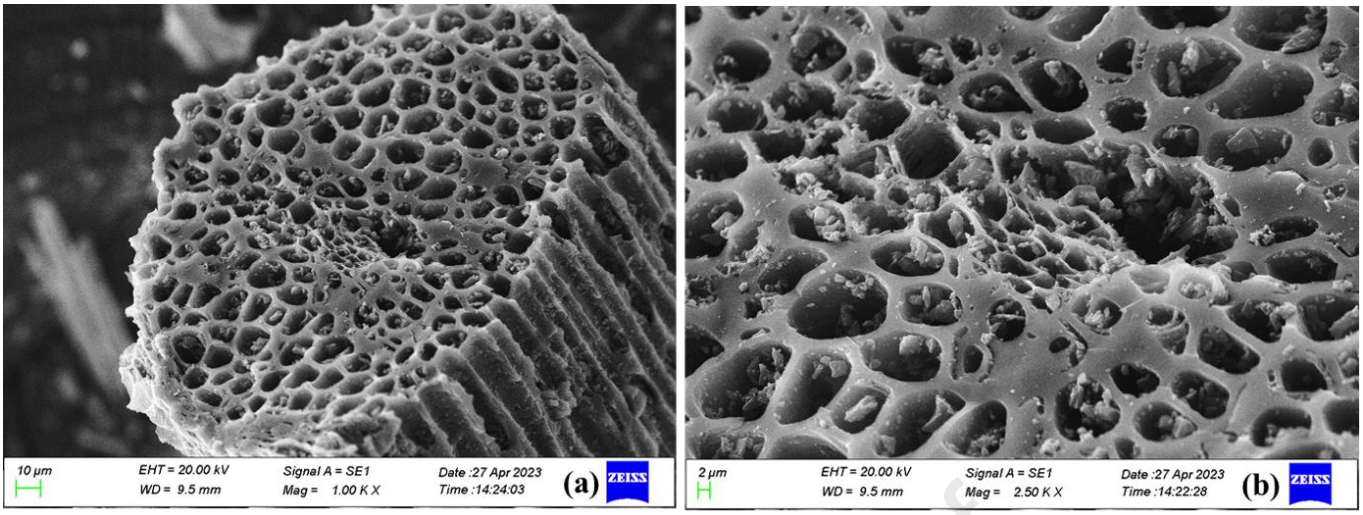

Figure 1. (a) and (b) SEM images of KBC800-HCl

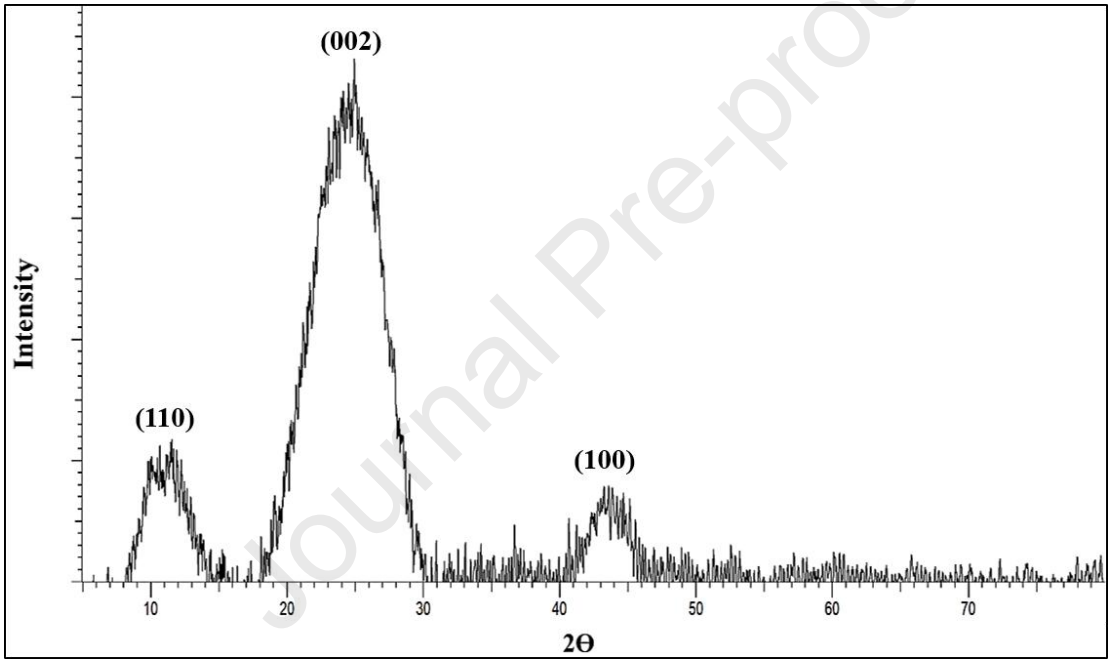

Figure 2. Diffractogram of KBC800-HCl

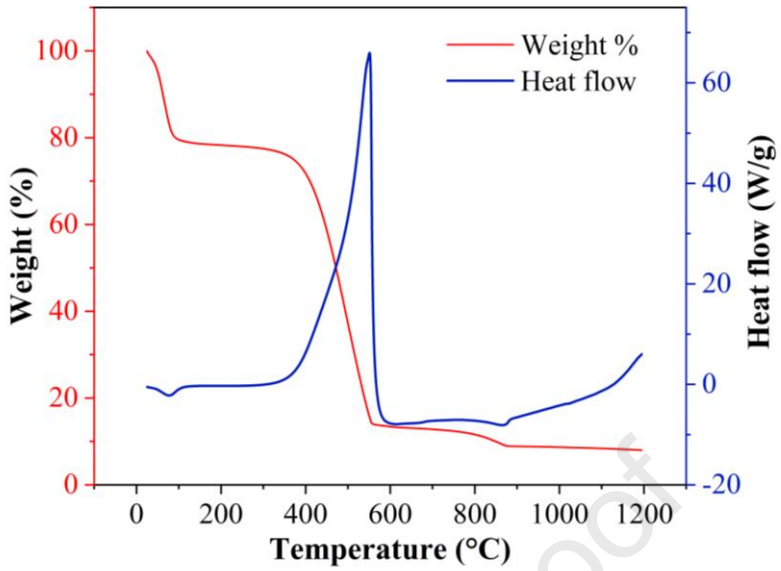

Figure 3. DSC-TGA curve of KBC800-HCl under a nitrogen atmosphere at a 10 °C/min heating rate

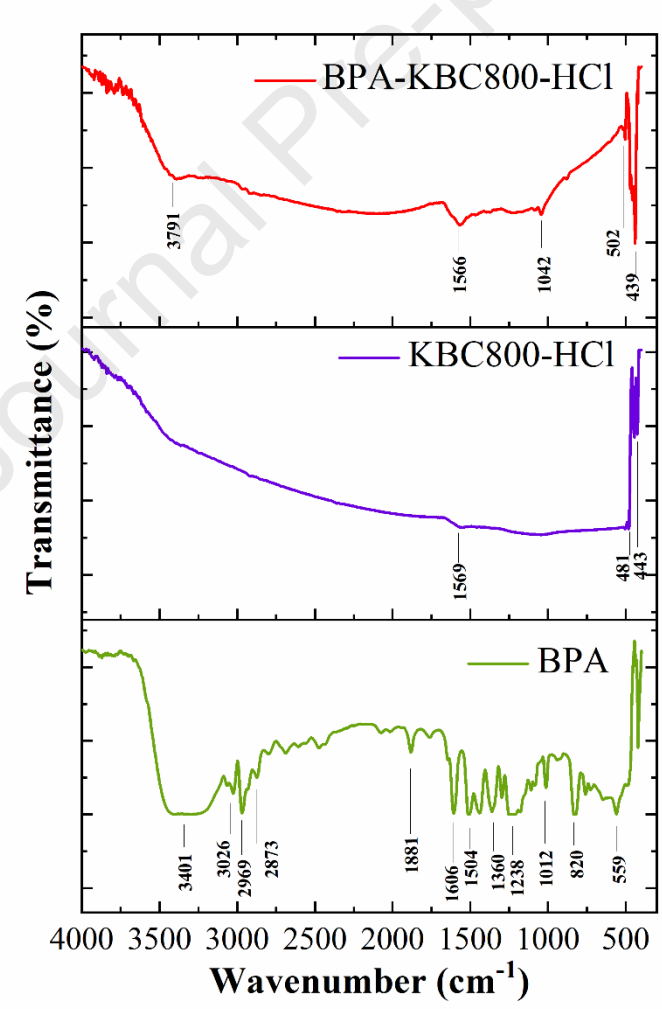

Figure 4. FTIR spectra of BPA, KBC800-HCl and BPA-KBC800-HCl

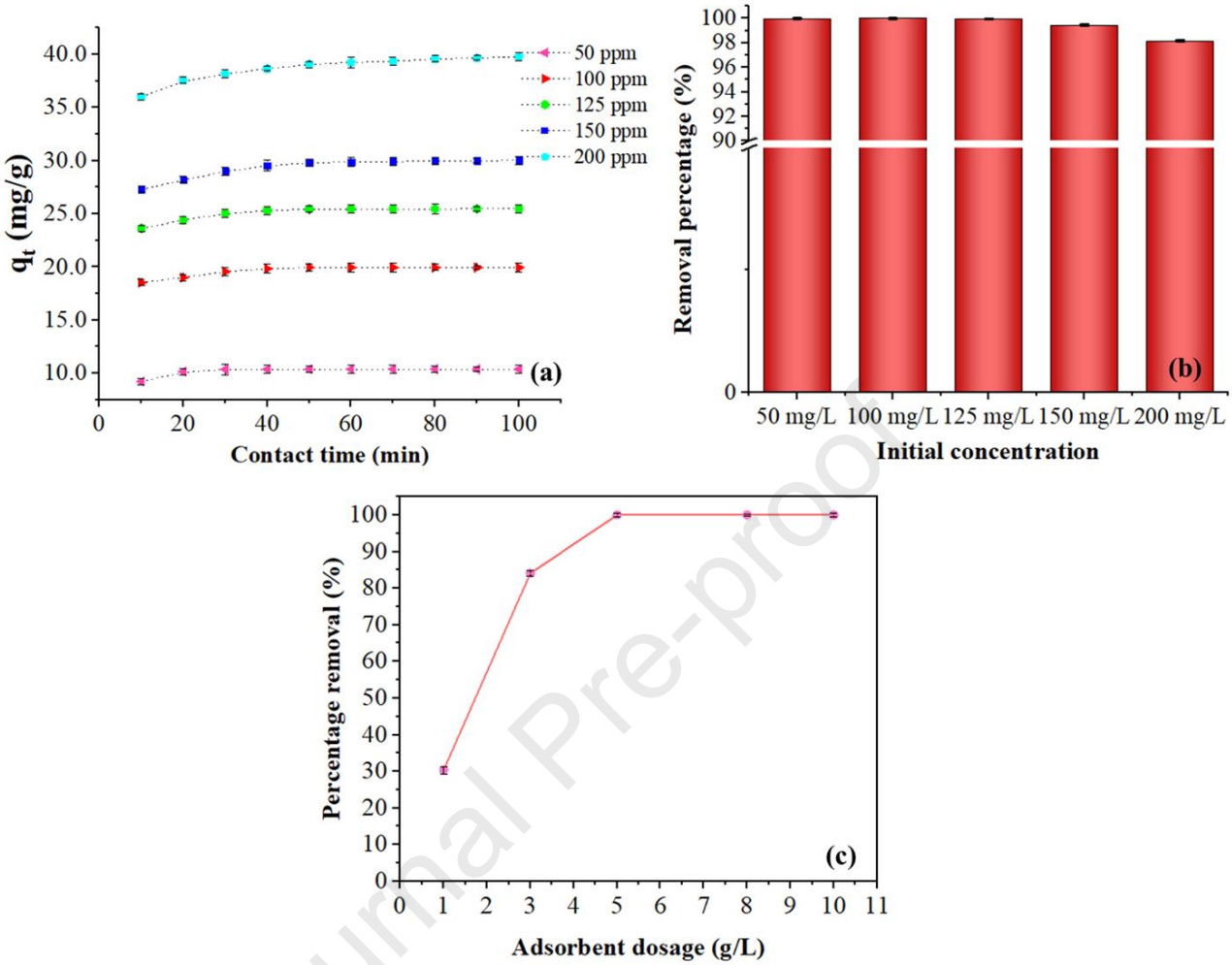

Figure 5. (a) Amount of BPA adsorbed at different initial concentrations and contact time, (b) Effect of initial concentration on BPA removal, (c) Effect of adsorbent dosage on BPA removal (C_0 = 100 mg/L, contact time: 60 min)

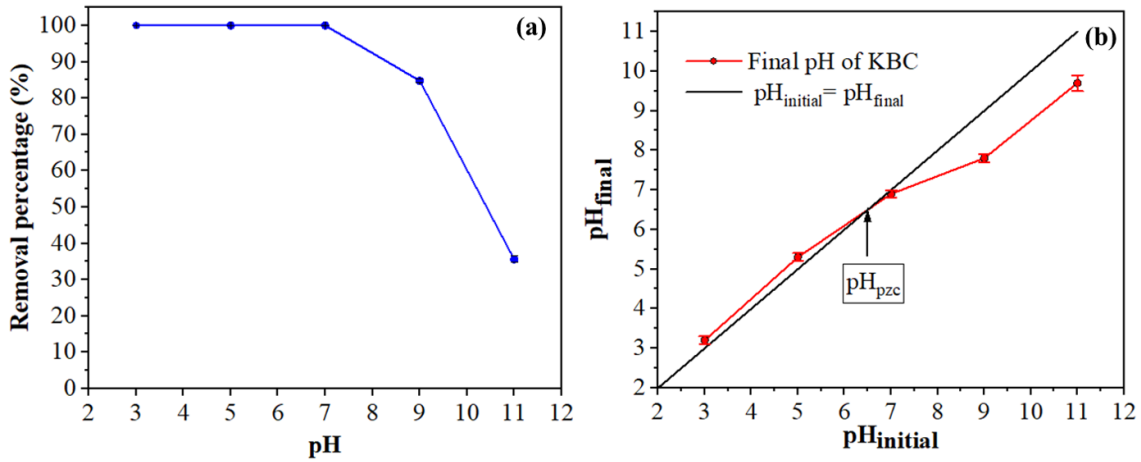

Figure 6. (a) Effect of solution pH on BPA removal (C_0 = 100 mg/L, contact time: 60 min, adsorbent dosage = 5 g/L), (b) Point of zero charge (pH_{PZC}) of KBC800-HCl

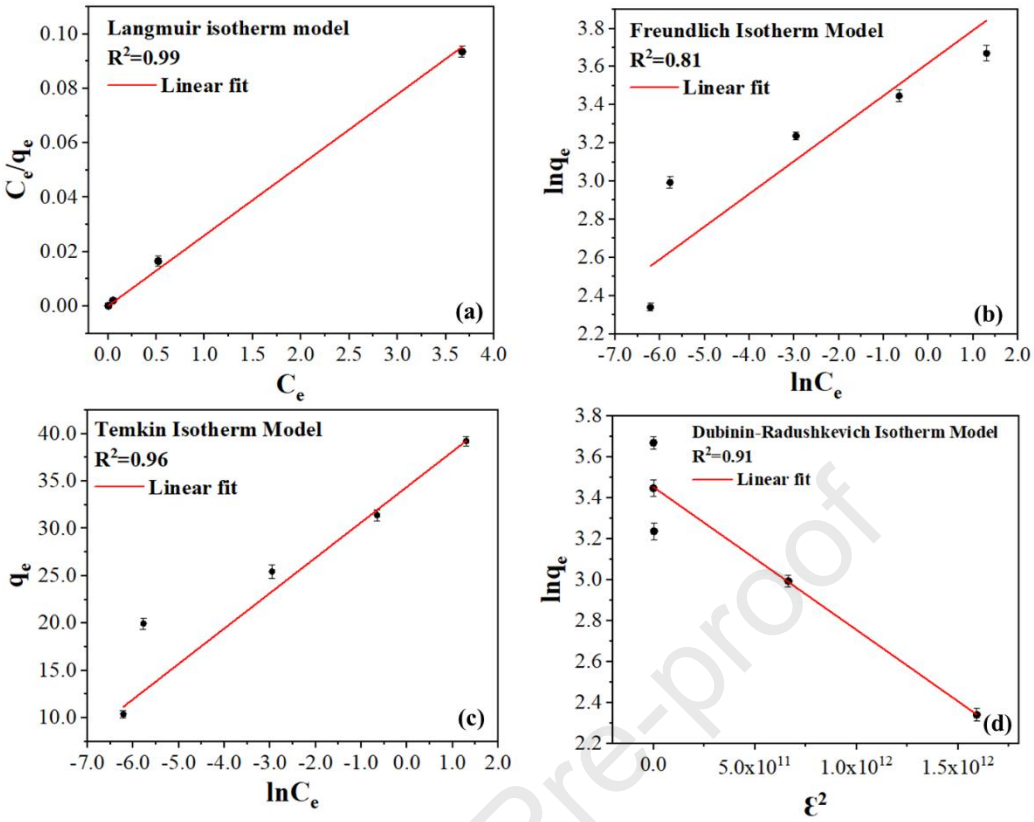

Figure 7. Adsorption isotherm models of KBC800-HCl (a) Langmuir (b) Freundlich (c) Temkin and (d) Dubinin-Radushkevich

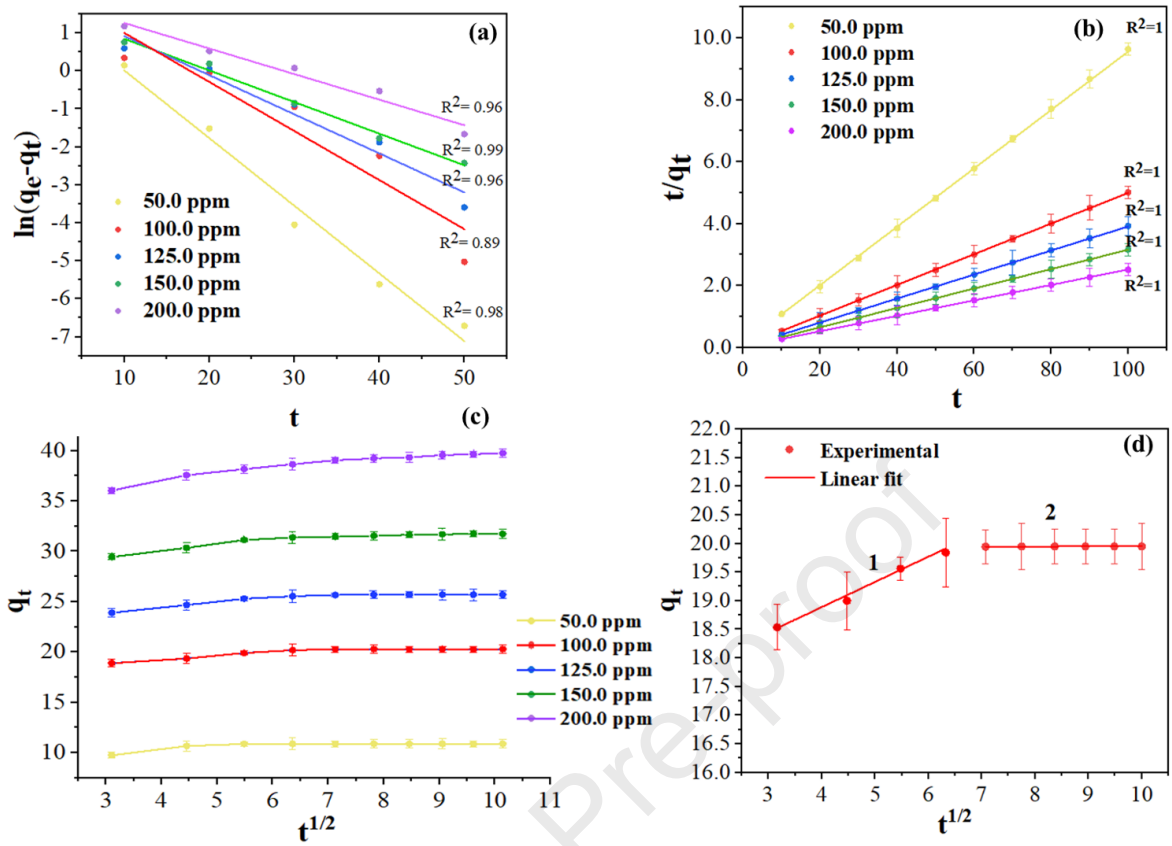

Figure 8. Kinetic models for BPA adsorption on KBC800-HCl (a) Pseudo-first-order (b) Pseudo-second-order (c) Intraparticle diffusion model obtained under various initial concentrations of BPA (d) Intraparticle diffusion model at C_0 = 100.0 mg/L

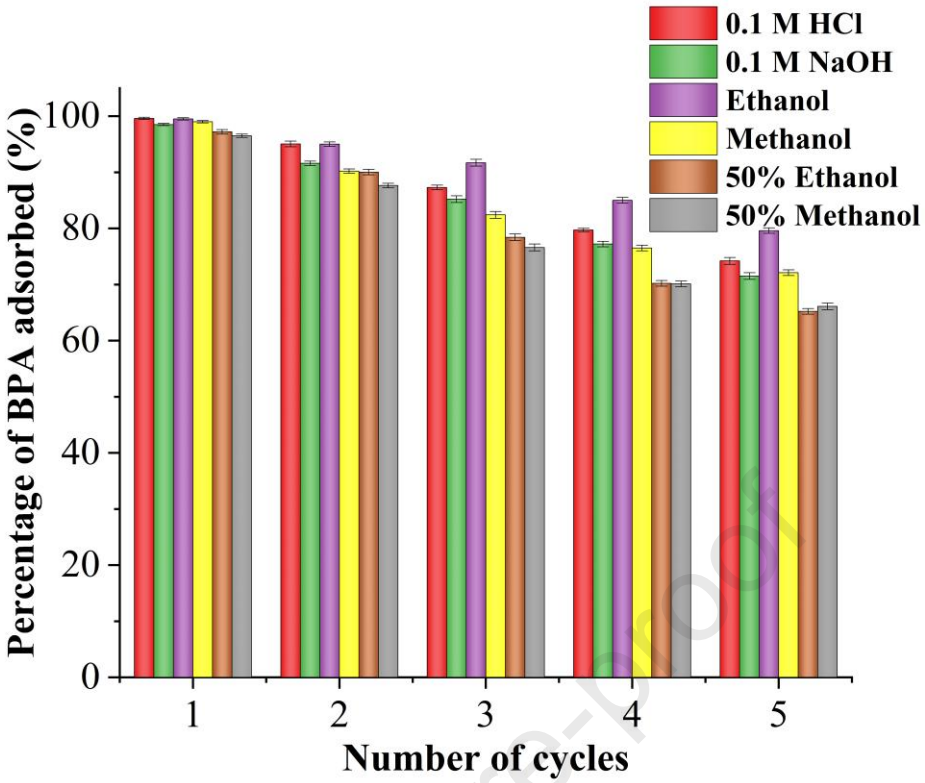

Figure 9. Percentage of BPA adsorption by KBC800-HCl with different eluting agents

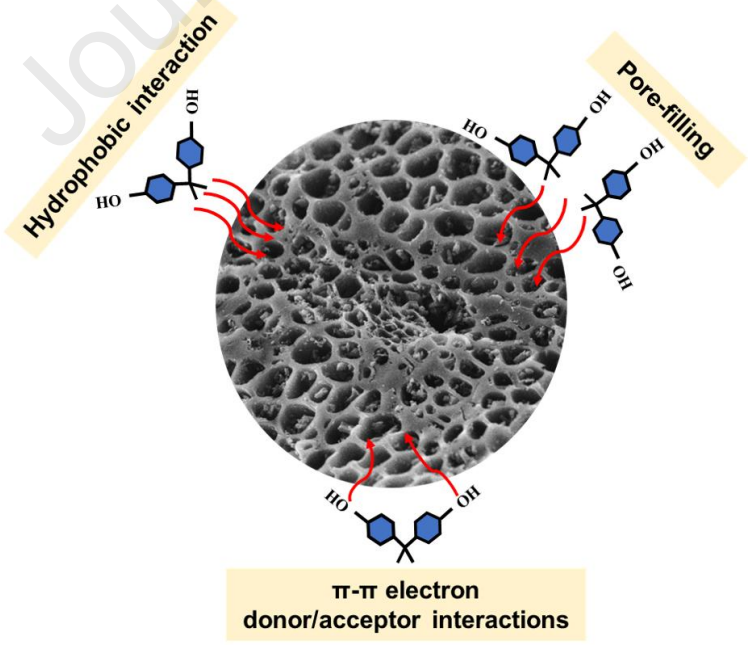

Figure 10. Possible adsorption mechanism of BPA onto KBC800-HCl

Declaration of interests

☒ The authors declare that they have no known competing financial interests or personal relationships that could have appeared to influence the work reported in this paper.

☐The authors declare the following financial interests/personal relationships which may be considered as potential competing interests: